Solid phase transitions in the liquid limit*

Yury Grabovsky† Lev Truskinovsky‡

Dedicated to the memory of Jerry Ericksen, a wizard

Abstract

We address the fundamental difference between solid-solid and liquid-liquid phase transitions within the Ericksen's nonlinear elasticity paradigm. To highlight ideas, we consider the simplest nontrivial 2D problem and work with a prototypical two-phase Hadamard material which allows one to weaken the rigidity and explore the nature of solid-solid phase transitions in a "near-liquid" limit. In the language of calculus of variations we probe limits of quasiconvexity in an "almost liquid" solid by comparing the thresholds for cooperative (laminate based) and non-cooperative (inclusion based) nucleation. Using these two types of nucleation tests we obtain for our model material surprisingly tight two-sided bounds on the elastic binodal without directly computing the quasiconvex envelope.

1 Introduction

In 1975 J. Ericksen posed for the first time the problem of solid-solid phase transitions in the framework of nonlinear elasticity theory. He effectively reformulated the classical physics question as a problem of vectorial calculus of variations. The contemporaneous theory viewed non-hydrostatically stressed solids as metastable and therefore did not distinguish between solid-solid and liquid-liquid phase transitions. Ericksen's insight that during phase transitions the non-hydrostatic stresses may persist at time scales of interest, revolutionized elasticity theory and initiated the extremely successful research program of studying materials with non-quasiconvex energies [44, 13, 37, 6, 10]. The goal of the present paper is to elucidate the difference between solid-solid and liquid-liquid phase transitions within the Ericksen's nonlinear elasticity paradigm.

From the perspective of elasticity theory, the main difference between liquids and solids is that liquids do not resist shear [8, 14]. This degeneracy in the elastic constitutive structure of liquids is responsible for their peculiar behavior during first order phase transitions vis-à-vis the behavior of solids, characterized by finite rigidity [21]. For both solids and liquids, reaching phase equilibrium often means the formation of phase mixtures. However, while

*J. Elast., No. 155, pp. 717–745, 2024

†Department of Mathematics, Temple University, Philadelphia, PA 19122, USA

‡PMMH, CNRS – UMR 7636, ESPCI, PSL, 75005 Paris, France

the phase organization in liquid phase transitions is largely controlled by surface tension, in solid phase transitions the dominance of elastic long-range interactions leaves to surface tension only a minor role of a scale selection. The dependence of energy on the geometric arrangement of the phases in solids leads to specific morphologies, largely controlled by the interplay between the location of the energy wells and their kinematic compatibility [5].

First order phase transitions in liquids are well understood at both physical and mathematical levels [39, 13]. The reason is that the scalar problem confronted in the liquid case is fully solvable [11]. Instead, despite many dedicated efforts, largely inspired by the pioneering contributions of Ericksen himself [16, 15, 17, 18, 19], the mathematical understanding of elastic phase transitions in solids is still far from being complete. In particular, some basic underlying vectorial problems of the calculus of variations remain unsolved [6, 3].

To set the stage, we recall that in nonlinear elasticity the energy functional can be written in the form $E[\boldsymbol{y}] = \int_\Omega W(\nabla \boldsymbol{y}) d\boldsymbol{x}$, where $W(\boldsymbol{F})$ is the energy density function describing the elastic properties of the material. For the energy minimizing configurations the physically informed energy density $W(\boldsymbol{F})$ can be replaced by its quasiconvexification $QW(\boldsymbol{F})$ [12]. The latter can be given by an implicit formula which becomes explicit only if one knows the energy minimizing microstructures. In the case of liquids the geometry of such microstructures is irrelevant and the construction of $QW(\boldsymbol{F})$ reduces to convexification. In the case of solids, the task of finding the equilibrium microstructures in a generic setting is daunting.

With the aim of building a bridge between elastic phase transitions in liquids and solids, we consider in this paper a special limit of "near-liquid" solids which are characterized by an arbitrarily weak resistance to shear. We pose the general question of how in such a limit the tight control on the geometry of optimal microstructures by elastic interactions is lost. To answer this question we address a simpler problem of describing in this limit the boundary of the set of stable single-phase configurations. Such problem can be solved in the case of "strongly-solid" elastic phase transitions when the equilibrium microstructures are simple laminates [27]. The goal of the present paper is to understand the opposite, "weakly-solid" limit, when the simplest laminate-based microstructures are clearly suboptimal.

In physics literature the boundary of the set of stable single-phase configurations is delineated by the classical Maxwell-Gibbs equilibrium conditions which were originally developed to describe phase equilibrium in liquids [41, 20]. These conditions allow one to identify the homogeneous configurations that are unstable to perturbations that are small in extent but not necessarily in magnitude. Such configurations are known in physics as constituting the binodal region [45]. In the mathematical theory of elastic phase transitions, the "solid" analog of the binodal region would incorporate the homogeneous states that fail to be strong local minima of the energy functional.

In this perspective, the binodal region is a subset in the configuration space of strain measures where the quasiconvex envelope lies below the energy density. Locating the boundary of the binodal region (called the *binodal* in physics) in the general setting constitutes a major challenge. While remaining nontrivial, this task appears, at least a priori, as more tractable than the task of constructing the actual quasiconvex envelope. In the present paper we address the problem of the binodal in the "near-liquid" case and show that in this limit the explicit knowledge of the binodal can lead directly to explicit formulas

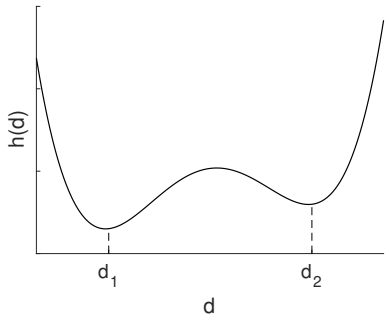

Figure 1: Double-well structure of the energy density $h(d)$.

for at least some parts of the quasiconvex envelope.

In our prior work we have developed general methods for identifying subsets of the binodal marking the emergence (nucleation) of coherent regions of a new phase [24]. The main tool in such analysis is the characterization of the jump set [23]—a codimension one variety in the phase space corresponding to nucleation of coherent laminae. The knowledge of the jump set provides a general way to constrain (bound) the binodal from within, without any guarantee that the bound is optimal. Applying our methods of identifying both stable and unstable parts of the jump set ultimately leads to a realistic approximation of the whole binodal in the "near-liquid" limit.

To highlight ideas, we focus in this paper on the simplest family of non-quasiconvex energy densities describing Hadamard materials [31, 32]: $W(\boldsymbol{F}) = \frac{\mu}{2}|\boldsymbol{F}|^2 + h(\det \boldsymbol{F})$. Specifically, we are interested in the case of two space dimensions[1] and assume that the function $h(d)$ describes a generic double-well potential modeling isotropic-to-isotropic phase transition (see Fig. 1). The main advantage of this class of energy densities is that it contains a single parameter μ which can be viewed as a scale of the effective rigidity. By varying this scale one can study the entire range of intermediate rigidity responses from "strong" ($\mu \gg 1$) to "weak" ($\mu \ll 1$) and in this way expose the crossover from "solid" to "liquid" behavior.

An interesting property of Hadamard materials is the subtle *asymmetry* between the two isotropic phases. It is intriguing, as it can be attributed neither to the difference between the elastic moduli of the phases nor to the geometric nonlinearity of the model. Indeed, it persists even if the two wells of the nonlinear potential $h(d)$ are identical in the sense that they have the same height and the same tangential elastic moduli. The only difference between the two phases is then governed by the small term $\mu|\boldsymbol{F}|^2/2$, that is larger at the low density phase and smaller at the high density phase. However, due to this difference, and in contrast to the case of an ostensibly similar geometrically linearly model [35, 43, 36], the two phases of an Hadamard material admit rather dissimilar ecosystems of instability mechanisms. Thus, rather remarkably, the instability of the low energy phase proceeds by nucleation of a compact region of the high energy minority phase, in contrast to the formation of laminar microstructure, when the high energy phase loses its stability. We

[1] In principle, our methodology is also applicable in 3D. In this paper we have chosen a 2D setting to make the ideas and techniques fully transparent and to be able to illustrate them graphically.

show that such an asymmetry leads to a coexistence of "strongly-solid" and "weakly-solid" (or even "quasi-liquid") responses inside a single material model. In particular, even in the absence of hysteresis, the direct and reverse phase transitions in such material can proceed according to morphologically distinct transformation mechanisms.

To understand this behavior, we first recall that while for an Hadamard material the double well energy structure is described in terms of a single scalar potential $h(d)$, the results of relaxation of $W(\boldsymbol{F})$ are nontrivial due to the inherent incompatibility of the energy wells, which is in turn associated with the purely volumetric nature of the phase transition. In the case of only one well, when the phase transition is absent, the result of such relaxation is trivial as it is known that $W(\boldsymbol{F})$ is quasiconvex if and only if $h(d)$ is convex [4]. The relaxation of $W(\boldsymbol{F})$ with two wells and non-convex $h(d)$ is known for the "infinitely-weak" solids (effectively liquids) with $\mu = 0$, where $QW(\boldsymbol{F}) = h^{**}(\det \boldsymbol{F})$ [11] and in the "strongly-solid" limit when the shear modulus μ is sufficiently large [27]. In the latter case the quadratic term in the energy dominates the double-well term and the formula for $QW(\boldsymbol{F})$ couples $|\boldsymbol{F}|$ and $\det \boldsymbol{F}$ placing the relaxed energy between $W(\boldsymbol{F})$ above and $U(\boldsymbol{F}) = \frac{\mu}{2}|\boldsymbol{F}|^2 + h^{**}(\det \boldsymbol{F})$ below.

In the present paper we show that the lower bound on the rigidity measure μ in [27] was not a technical limitation, and that, as μ decreases, the above "strongly-solid" expression for $QW(\boldsymbol{F})$ ceases to be valid in the subsets of the binodal corresponding to hydrostatic Dirichlet boundary conditions. More specifically, we show that in the limit of small μ, the relaxation of $W(\boldsymbol{F})$ goes through a chain of structural transitions with simple lamination persisting either for high shear loading or in the vicinity of the higher energy well. Close to the low energy well it is replaced by more complex optimal microstructures which remain not fully characterized. Fig. 2 shows the schematic energy landscape of the Hadamard material in the variables $\det \boldsymbol{U} = \varepsilon_1\varepsilon_2$, and $\mathrm{dev}(\boldsymbol{U}) = \varepsilon_1 - \varepsilon_2$, where $\boldsymbol{U} = (\boldsymbol{F}^T\boldsymbol{F})^{1/2}$ and ε_1 and ε_2 are the singular values of the deformation gradient $\boldsymbol{F}$; in both panels the black dot represents the applied affine hydrostatic Dirichlet boundary conditions. The left panel shows the fields and their rank-one connections at the onset of the instability of the high energy phase. The compatible field (inside a simple laminate) takes two values represented by the red dot on the left and one of the two red dots on the right. The right panel shows the fields at the onset of the instability in the low energy phase. The corresponding compatible field takes values in the set represented by the red dot on the left and the red segment on the right. Here the system takes advantage of a shallow valley (μ is small) which provides an opportunity to accommodate the loading through low energy elastic deformation (remotely reminiscent of a fluid flow). Note, however, that the emergence of different types of instability mechanisms along direct and return deformation paths cannot be attributed solely to geometric nonlinearity of the Hadamard model, as a somewhat similar asymmetry is also present in the geometrically linear model whenever the two phases have different well ordered elastic moduli: in that case the material with larger elastic moduli plays the role of the high energy phase [1, 22, 9, 2].

In this paper our main technical approach is to generate bounds on the binodal surface. The simplest bounds are obtained as a result of probing the binodal by means of nucleating first rank laminates. Their optimality is proved by establishing their polyconvexity (and therefore quasiconvexity); the corresponding problem is algebraic because the supporting

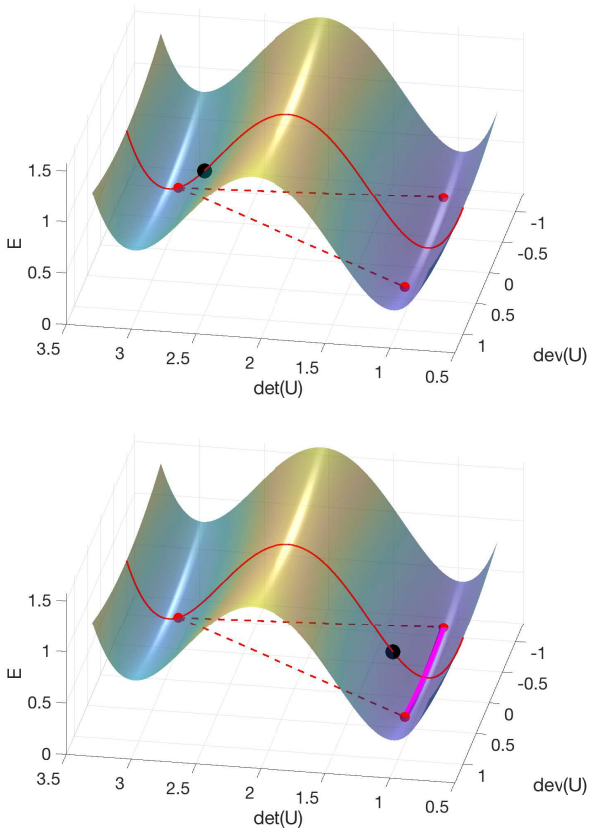

Figure 2: The schematic energy landscape of the Hadamard material showing the elastic fields at the point of instability of the homogeneous state (incipient phase transition). Left panel: instability of the high energy phase. Right panel: instability of the low energy phase. The initial state is represented by a black dot.

null-Lagrangians can be constructed explicitly [28]. In contrast with the "strongly solid" regime of large μ, in the "near-liquid" regime of small μ, not all of the constructed first rank laminate bounds turn out to be optimal.

The simple laminate bounds are first improved by considering the nucleation of second rank laminates even though, as will be shown in [30], the second rank laminate bounds are also not optimal, hinting instead towards a possible optimality of infinite rank laminates. We could improve them analytically (for hydrostatic strains only) by considering nucleation of a bounded circular inclusion in the infinite plane. Moreover, we provided a rationale behind the conjecture that the "circular inclusion bound" is in fact optimal. We show that if this conjecture could be proved, the the values of the deformation gradient in the exterior of the circular nucleus would provide a bound on the whole binodal from the outside of the binodal region. Another consequence of the conjectured optimality of the inclusion-based nucleation bound would be the explicit formula for the quasiconvex envelope $QW(\boldsymbol{F})$ at all hydrostatic strains. To corroborate our conjecture we juxtaposed the results obtained for bounded inclusions and unbounded second rank laminates and derived tight two-sided bounds on the binodal. As will be reported elsewhere, numerical computations show that

both bounds remain tight in the full range of parameters for which they are meaningful, with the hypothetical bound being in perfect agreement with the numerically computed rank-one convex binodal.

The paper is organized as follows. In Section 2 we recapitulate the relevant results from the calculus of variations for nonconvex vectorial problems which are later used in the paper. In Section 3 we specialize these results for the Hadamard material and present the numerical illustrations of the obtained bounds. Analytical results for the limiting case $\mu \to 0$ are presented in Section 4 where we also illustrate them with numerical computations. In Section 5 we demonstrate the far reaching consequences of the assumed optimality of the nucleation bound. The paper ends with a general discussion and conclusions in Section 6.

2 Preliminaries

Binodal region. We recall that hyperelastic materials in an n-dimensional space are characterized by the following form of the energy stored in the deformed elastic body

$$E[\boldsymbol{y}] = \int_\Omega W(\nabla \boldsymbol{y}(\boldsymbol{x}))d\boldsymbol{x}.$$

Here $\Omega \subset \mathbb{R}^n$ is the reference configuration, and $\boldsymbol{y} : \Omega \to \mathbb{R}^n$ is the deformation. To deal with stable (i.e. experimentally observable) configurations of the body one can replace the energy density $W(\boldsymbol{F})$ with a relaxed one $QW(\boldsymbol{F})$, known as a quasiconvexification of $W(\boldsymbol{F})$. Even though, there is a formula for $QW(\boldsymbol{F})$ [12]:

$$QW(\boldsymbol{F}) = \inf_{\boldsymbol{\phi} \in C_0^\infty(B;\mathbb{R}^n)} \frac{1}{|D|} \int_B W(\boldsymbol{F} + \nabla \boldsymbol{\phi})d\boldsymbol{x}, \tag{2.1}$$

where B is the unit ball, there are no systematic approaches to actually compute it.

A simpler, but just as useful an object, is the elastic binodal.

Definition 2.1. *An elastic binodal is the boundary of the binodal region*

$$\mathfrak{B} = \{\boldsymbol{F} : QW(\boldsymbol{F}) < W(\boldsymbol{F})\}. \tag{2.2}$$

Definition 2.2. *We say that the matrix $\boldsymbol{F}$ is stable, if $W(\boldsymbol{F}) = QW(\boldsymbol{F})$.*

Thus, the binodal is the surface separating the binodal region from the set of stable configurations.

Jump set. While there exist rank-one convex, non quasiconvex functions, most cases of practical interest in elastic phase transitions feature multiwell energies that are not rank-one convex. Such functions possess a non-trivial *jump set*, stable points of which form a part of the binodal (or even the entire binodal). The jump set is the set of solutions $\boldsymbol{F} = \boldsymbol{F}_-$ of the equations [23]

$$\begin{cases} \boldsymbol{F}_+ = \boldsymbol{F}_- + \boldsymbol{a} \otimes \boldsymbol{n}, \\ [\![\boldsymbol{P}]\!]\boldsymbol{n} = 0, \\ [\![\boldsymbol{P}^T]\!]\boldsymbol{a} = 0, \\ [\![W]\!] - \langle \{\!\{ \boldsymbol{P} \}\!\}, [\![\boldsymbol{F}]\!] \rangle = 0, \end{cases} \tag{2.3}$$

where $\boldsymbol{a} \neq 0$, $|\boldsymbol{n}| = 1$, and the following standard notations are used.

$$\boldsymbol{P}_\pm = W_{\boldsymbol{F}}(\boldsymbol{F}_\pm), \quad [\![\boldsymbol{F}]\!] = \boldsymbol{F}_+ - \boldsymbol{F}_-, \quad \{\!\{\boldsymbol{P}\}\!\} = \frac{\boldsymbol{P}_+ + \boldsymbol{P}_-}{2}, \quad \langle \boldsymbol{A}, \boldsymbol{B} \rangle = \operatorname{Tr}(\boldsymbol{A}\boldsymbol{B}^T),$$

where $W_{\boldsymbol{F}}$ indicates the matrix of partial derivatives $P_{ij} = \partial W / \partial F_{ij}$. The vectors $\boldsymbol{a}$ and $\boldsymbol{n}$ can be eliminated from (2.3), leaving a single scalar equation for $\boldsymbol{F}$ that describes the jump set. The points on the jump set belong either to the binodal or to the binodal region $\mathfrak{B}$, see [23] for details. Hence, the jump set always represents a bound on the binodal region from within.

One of the constructive ways to detect the unstable parts of the jump set is to use the Weierstrass condition, which is necessary for stability,

$$W^\circ(\boldsymbol{F}, \boldsymbol{b} \otimes \boldsymbol{m}) \geq 0, \quad \forall \boldsymbol{b} \in \mathbb{R}^n, \ |\boldsymbol{m}| = 1, \tag{2.4}$$

where

$$W^\circ(\boldsymbol{F}, \boldsymbol{H}) = W(\boldsymbol{F} + \boldsymbol{H}) - W(\boldsymbol{F}) - \langle W_{\boldsymbol{F}}(\boldsymbol{F}), \boldsymbol{H} \rangle.$$

We have proved in [25] that the pairs of points $\boldsymbol{F}_\pm$ on the jump set are either both stable or both unstable. Hence, a point $\boldsymbol{F}_+$ satisfying (2.4) can be still classified as unstable, if $\boldsymbol{F}_-$ fails (2.4). While there are other conditions of stability that don't follow from (2.4) (see [26]) we will only make use of an easily verifiable corollary of (2.4) that restricts the rank-one test fields $\boldsymbol{b} \otimes \boldsymbol{m}$ to an infinitesimally small neighborhood of $[\![\boldsymbol{F}]\!] = \boldsymbol{a} \otimes \boldsymbol{n}$ (see [23, (4.5)]).

Currently, the only general tool for establishing stability of an affine configuration $\boldsymbol{F}$ is by proving polyconvexity of W at $\boldsymbol{F}$, which is sufficient but rather far from necessary. In two dimensions it reduces to finding a constant $m \in \mathbb{R}$, such that

$$W^\circ(\boldsymbol{F}, \boldsymbol{H}) - m \det \boldsymbol{H} \geq 0, \qquad \forall \boldsymbol{H} \in \mathbb{R}^{2\times 2}. \tag{2.5}$$

If (2.5) holds, then $\boldsymbol{F}$ is stable in the sense of Definition 2.2. As shown in [28], for points $\boldsymbol{F}_\pm$ on the jump set the only value of m that could possibly work is,

$$m = \frac{\langle [\![\boldsymbol{P}]\!], \operatorname{cof} [\![\boldsymbol{F}]\!] \rangle}{|[\![\boldsymbol{F}]\!]|^2}. \tag{2.6}$$

Secondary jump set. The jump set described by (2.3) identifies the points on the binodal corresponding to nucleation of a layer of the new phase in the infinite domain occupied by the original phase. As we have already mentioned, the entire jump set lies in the closure of the binodal region [23] and as such represents a bound on the binodal from the inside. Another such bound is provided by testing stability of the homogeneous phase with respect to nucleation of a twinned layer, or a second rank laminate. Mathematically, we can treat it as a jump set of a partially relaxed energy $\overline{W}$, defined by $\overline{W}(\overline{\boldsymbol{F}}) = \lambda W(\boldsymbol{F}_+) + (1-\lambda) W(\boldsymbol{F}_-)$, where $\overline{\boldsymbol{F}} = \lambda \boldsymbol{F}_+ + (1-\lambda)\boldsymbol{F}_-$, and where $\boldsymbol{F}_\pm$ is the corresponding pair on the jump set. Thus, the secondary jump set is defined by the system of equations

$$\begin{cases} \boldsymbol{F} = \overline{\boldsymbol{F}} + \boldsymbol{b} \otimes \boldsymbol{m}, \\ \boldsymbol{P}\boldsymbol{m} = \overline{\boldsymbol{P}}\boldsymbol{m}, \\ \boldsymbol{P}^T\boldsymbol{b} = \overline{\boldsymbol{P}}^T\boldsymbol{b}, \\ W(\boldsymbol{F}) - \overline{W} = \boldsymbol{P}\boldsymbol{m} \cdot \boldsymbol{b}, \end{cases} \tag{2.7}$$

where

$$\overline{W} = \lambda W(\boldsymbol{F}_+) + (1-\lambda)W(\boldsymbol{F}_-), \qquad \overline{\boldsymbol{P}} = \lambda \boldsymbol{P}_+ + (1-\lambda)\boldsymbol{P}_-, \tag{2.8}$$

for some $\lambda \in [0,1]$, which also plays the role of a variable to be solved for in (2.7), along with $\boldsymbol{F}$, $\boldsymbol{b} \neq 0$, and $|\boldsymbol{m}| = 1$.It is clear that the so defined secondary jump set represents another bound on the binodal region from within.

Nucleation criterion. Yet another method of probing the binodal is to study the nucleation of bounded inclusions either of a prescribed shape [7, 40, 38] or of an optimal shape which must be determined [33, 42, 34]. The theory justifying why these tests probe the binodal was developed in [24]. In the case of "nucleation of a bounded inclusion", the criterion for $\boldsymbol{F}_0$ to be "marginally stable", i.e. to lie in the closure of $\mathfrak{B}$, is the existence of a field

$$\boldsymbol{\phi} \in \mathcal{S} = \{\boldsymbol{\phi} \in L^2_{\rm loc}(\mathbb{R}^n) : \nabla\boldsymbol{\phi} \in L^2(\mathbb{R}^n;\mathbb{R}^n)\},$$

such that

$$\nabla \cdot \boldsymbol{P}(\boldsymbol{F}_0 + \nabla\boldsymbol{\phi}) = 0, \qquad \nabla \cdot \boldsymbol{P}^*(\boldsymbol{F}_0 + \nabla\boldsymbol{\phi}) = 0 \tag{2.9}$$

in the sense of distribution in $\mathbb{R}^n$, where

$$\boldsymbol{P}(\boldsymbol{F}) = W_{\boldsymbol{F}}(\boldsymbol{F}), \qquad \boldsymbol{P}^*(\boldsymbol{F}) = W(\boldsymbol{F})\boldsymbol{I}_n - \boldsymbol{F}^T\boldsymbol{P}(\boldsymbol{F}),$$

and where the solution $\boldsymbol{\phi}$ satisfies the non-degeneracy condition

$$\int_{\mathbb{R}^n} W^\circ_{\boldsymbol{F}}(\boldsymbol{F}_0, \nabla\boldsymbol{\phi}) d\boldsymbol{x} \neq 0. \tag{2.10}$$

In the case of nucleation of a bounded inclusion ω with smooth boundary the verification of (2.9) consists in checking that the field $\boldsymbol{\phi} \in \mathcal{S}$ solves $\nabla \cdot \boldsymbol{P}(\boldsymbol{F}_0 + \nabla\boldsymbol{\phi}) = 0$ both inside and outside of ω, together with the condition that the traces $\boldsymbol{F}_\pm(\boldsymbol{x}) = \boldsymbol{F}_0 + \nabla\boldsymbol{\phi}_\pm(\boldsymbol{x})$ on the two sides of $\partial\omega$ form a corresponding pair on the jump set for each $\boldsymbol{x} \in \partial\omega$. If, in addition, we can somehow prove that $\boldsymbol{F} + \nabla\boldsymbol{\phi}(\boldsymbol{x})$ is stable in the sense of Definition 2.2, for each $\boldsymbol{x} \in \mathbb{R}^n$, then $\boldsymbol{F}_0$ must lie on the binodal. Conversely, if it is known that $\boldsymbol{F}_0$ is stable, then all matrices $\boldsymbol{F}(\boldsymbol{x}) = \boldsymbol{F}_0 + \nabla\boldsymbol{\phi}(\boldsymbol{x})$ are stable for all $\boldsymbol{x} \in \mathbb{R}^n$.

3 The Hadamard material

In this paper we focus on a particularly simple, yet nontrivial energy

$$W(\boldsymbol{F}) = \frac{\mu}{2}|\boldsymbol{F}|^2 + h(d), \quad \boldsymbol{F} \in \{\boldsymbol{F} \in GL(n) : \det\boldsymbol{F} > 0\}, \quad d = \det\boldsymbol{F}, \tag{3.1}$$

where $h(d)$ is a $C^2(0,+\infty)$ function with a double-well shape. In our explicit computations and illustrations we use the quartic double-well energy[2]

$$h(d) = (d-d_1)^2(d-d_2)^2, \tag{3.2}$$

[2]Formula (3.2) only needs to hold in an arbitrary neighborhood of $[d_1, d_2]$. The potential $h(d)$ can be modified outside of that neighborhood arbitrarily, as long as $h^{**}(d) = h(d)$ there. In particular, the singular behavior of $h(d)$ as $d \to 0^+$, required in nonlinear elasticity, can be easily assured.

which affords certain simplification of general formulas. In this section we provide an approximation for the binodal of this energy, even though its quasiconvex envelope is not known. We begin with the computation of the jump set for this class of materials.

The jump set. In Appendix A we summarize, for the sake of completeness, the discussion of the jump set from [27], which is adapted here to our two-dimensional setting. The main result of the Appendix A is that the jump set of (3.1) consists of matrices $\boldsymbol{F}_\pm$, whose two singular values labelled[3] ε_0 and $\varepsilon_\pm$ satisfy the equations

$$\varepsilon_0[\![h']\!] + \mu[\![\varepsilon]\!] = 0, \quad [\![h]\!] - \{\!\{h'\}\!\}[\![d]\!] = 0, \quad d_\pm = \det \boldsymbol{F}_\pm = \varepsilon_0\varepsilon_\pm. \tag{3.3}$$

The first equation in (3.3) is equivalent to (A.4) if we recall the definition of $d_\pm$, given in the third equation in (3.3). Our notation reflects the fact that for each pair $\boldsymbol{F}_\pm$ on the jump set there is a frame in which both matrices are diagonal and share the same singular value ε_0 with the same eigenvector.

Equations (3.3) can be now used to derive the semi-explicit parametric equations of the jump set, with $d_+ = \varepsilon_0\varepsilon_+$, serving as a parameter. Given d_+ we can use the second equation in (3.3) to solve for d_-. This solution will be denoted $d_- = D(d_+)$. Multiplying the first equation in (3.3) by ε_0 we obtain the parametric equations

$$\begin{cases} \varepsilon_0(d_+) = \sqrt{-\frac{\mu[\![d]\!]}{[\![h']\!]}}, \\ \varepsilon_+(d_+) = \frac{d_+}{\varepsilon_0(d_+)}. \end{cases}$$

In the special case of potential (3.2) further simplifications can be made. For example,

$$[\![h]\!] - \{\!\{h'\}\!\}[\![d]\!] = [\![d]\!]^3(d_1 + d_2 - d_+ - d_-),$$

and therefore, $d_- = d_1 + d_2 - d_+ =: D(d_+)$. It then follows that

$$\{\!\{h'\}\!\} = 0, \qquad \varepsilon_+ + \varepsilon_- = \frac{d_1 + d_2}{\varepsilon_0}. \tag{3.4}$$

In particular, we can eliminate $h'(d_\pm)$ using (3.3) and (3.4) to obtain:

$$h'(d_\pm) = \{\!\{h'\}\!\} \pm \frac{1}{2}[\![h']\!] = \mp\frac{\mu}{2}\frac{[\![\varepsilon]\!]}{\varepsilon_0}. \tag{3.5}$$

Moreover, for quartic energy (3.2) we can write the equation of the jump set explicitly as $\varepsilon_\pm = \varepsilon_\pm(\varepsilon_0)$ where $\varepsilon_\pm = d_\pm/\varepsilon_0$, and $d_\pm$ solves

$$(d_\pm - d_1)(d_\pm - d_2) = -\frac{\mu}{4\varepsilon_0^2}. \tag{3.6}$$

The two roots of (3.6) are the values of $d_\pm$, where, by convention, we denote by d_+ the larger root. Equation (3.6) has exactly two real roots whenever $\varepsilon_0 > \sqrt{\mu}/(d_2 - d_1)$. Hence, explicitly,

$$\varepsilon_\pm = \frac{1}{2\varepsilon_0}\left(d_1 + d_2 \pm \sqrt{(d_2 - d_1)^2 - \frac{\mu}{\varepsilon_0^2}}\right), \qquad \varepsilon_0 \geq \frac{\sqrt{\mu}}{d_2 - d_1}. \tag{3.7}$$

[3]We use the notation $\pm$ to make two statements at the same time, one for the "+" sign, the other for the "−" sign. For example, our statement says that the matrix $\boldsymbol{F}_+$ has two singular values ε_0 and ε_+ and the matrix $\boldsymbol{F}_-$ has two singular values ε_0 and ε_-.

In our calculations we will use equations (3.5) to eliminate all occurrences of $h'(d_\pm)$ and equations (3.7) to eliminate $\varepsilon_\pm$, both uniquely determined by a single parameter ε_0.

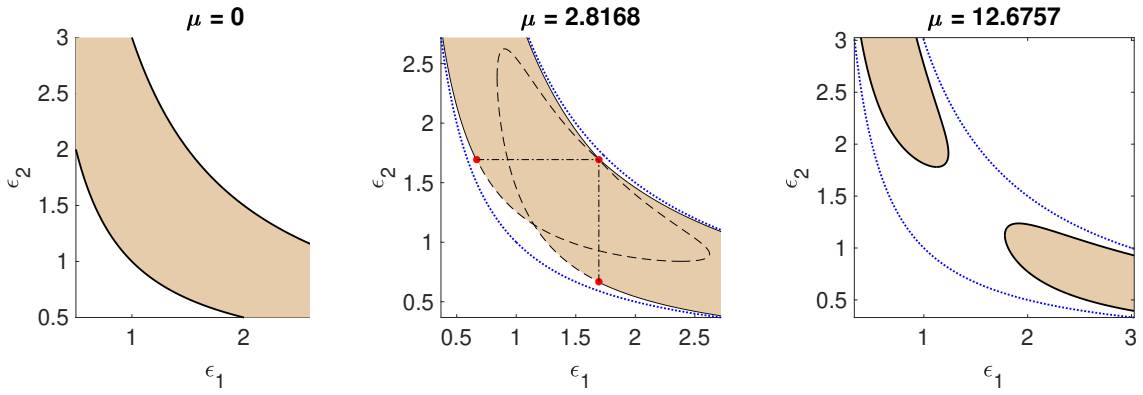

Figure 3: Jump sets in the case when $h(d)$ is given by (3.2) with $d_1 = 1$, $d_2 = 3$, and different values of μ. The convexification hyperbolas $\varepsilon_1\varepsilon_2 = d_{1,2}$ are shown by blue dotted lines. The bold black lines show stable part of the jump set. The dashed black lines represent the unstable part of the jump set. The W-points are represented by red dots and dashed-dotted lines show the rank-one connections between the W-points. The shaded region is the part of the binodal region delimited by the jump set. Its interior is unstable.

Numerical illustrations. When μ is sufficiently large the jump set is known to comprise the entire binodal [27]. Since each point of such binodal corresponds to the nucleation of a simple laminate, one immediately obtains an explicit formula for the relaxation $QW(\boldsymbol{F})$. However, as the shear modulus μ decreases, parts of the jump set may become unstable which will also affect the structure of $QW(\boldsymbol{F})$. To illustrate this point we show in Fig. 3 the jump sets in the case when $h(d)$ is given by (3.2), and the three different values of the shear modulus μ are chosen to be of the form $\mu = 0$, $\mu_{\text{top}}/3$, and $1.5\mu_{\text{top}}$, where μ_{top} is the largest value of μ for which the jump set has points of self-intersection. In Fig. 3 the dotted lines indicate "convexification hyperbolas", i.e., hyperbolas $\varepsilon_2 = d_1/\varepsilon_1$ and $\varepsilon_2 = d_2/\varepsilon_1$, where the interval $[d_1, d_2]$ is the interval on which $h(d)$ differs from its convex hull. The shaded region delimited by the jump set is unstable, while all points outside of the region bounded by the convexification hyperbolas are stable. It will be our main goal to specify the precise boundary of the unstable domain in the limit $\mu \to 0$.

W-points. In [26] we have shown that the easily computable corollary of the Weierstrass condition (2.4) for the energy (3.1) has the form

$$\varepsilon_0 \geq \varepsilon_\pm. \tag{3.8}$$

In [27] we have shown that this condition is always satisfied for large values of μ as is evident from the right panel in Fig. 3, while it has an obvious geometric interpretation in the middle panel in which the part of the jump set failing (3.8) is shown as a dashed line. The points marked by red dots in Fig. 3 that delimit the part of the jump set satisfying (3.8) will be called the Weierstrass points or W-points, for short. It will be shown in [30] that the solid portion of the jump set delimited by W-points is polyconvex for all sufficiently small μ.

Polyconvexity of W-points. By their nature W-points are either unstable or delimit the boundary of stability of the jump set. Our intuition, to be justified in [30], is that the larger the shear component of a point on the jump set the more stable it is. Thus, the range of μ for which W-points are polyconvex is also the range of μ for which the part of the jump set with larger shear, delimited by W-points is polyconvex.

One can provide an almost explicit characterization of all values of μ for which W-points are also points of polyconvexity assuming the quartic nonlinearity (3.2). Indeed, as discussed above, in order to prove the polyconvexity of W-points we need to establish (2.5), where m is given by (2.6). This problem has been already analyzed in [27], and we briefly summarize here the obtained results for the sake of completeness.

Establishing (2.5) for the energy (3.1) is equivalent to showing that

$$\Psi(\boldsymbol{F}) = \frac{\mu}{2}|\boldsymbol{F} - \boldsymbol{F}_\pm|^2 + h(\det \boldsymbol{F}) - h_\pm - h'_\pm\langle \operatorname{cof}\boldsymbol{F}_\pm, \boldsymbol{F} - \boldsymbol{F}_\pm\rangle - m\det(\boldsymbol{F} - \boldsymbol{F}_\pm) \tag{3.9}$$

is globally minimized by $\boldsymbol{F}_\pm$. Our notation in (3.9) emphasizes the fact that either choice of sign in $\boldsymbol{F}_\pm$ results in one and the same function $\Psi(\boldsymbol{F})$.

We first observed that the minimizer of $\Psi(\boldsymbol{F})$ must be a critical point, since $\Psi(\boldsymbol{F}) \to +\infty$, when $|\boldsymbol{F}| \to \infty$. We then showed that at all points on the jump set, except the points of self-intersection, the critical points $\boldsymbol{F}$ must be diagonal in the same frame as $\boldsymbol{F}_\pm$. Denoting by x and y the two diagonal entries of $\boldsymbol{F}$ we obtain

$$\Psi(\boldsymbol{F}) = \Phi(x, y) + \text{const},$$

where

$$\Phi(x,y) = \frac{\mu}{2}(x^2 + y^2) - \alpha x - \beta y + h(xy) - mxy,$$
$$\alpha = \mu(\varepsilon_+ + \varepsilon_-), \quad \beta = \mu\left(\varepsilon_0 + \frac{\varepsilon_+\varepsilon_-}{\varepsilon_0}\right), \quad m = \frac{[\![h'd]\!]}{[\![d]\!]}. \tag{3.10}$$

When we minimized $\Phi(x, y)$ over all (x, y), such that $xy = d$ we concluded that the minimizer is $(d/y, y)$, where $y = y(d)$ is the largest root of

$$y^4 - \beta_0 y^3 + d\alpha_0 y - d^2 = 0, \quad \alpha_0 = \varepsilon_+ + \varepsilon_-, \quad \beta_0 = \varepsilon_0 + \frac{\varepsilon_+\varepsilon_-}{\varepsilon_0}. \tag{3.11}$$

Thus, the minimum of $\Phi(x, y)$ is achieved at a finite point corresponding to a critical point of $\phi(d) = \Phi(d/y(d), y(d))$.

In the special case of W-points we have[4] $\varepsilon_+ = \varepsilon_0$ and therefore $\alpha_0 = \beta_0 = \varepsilon_- + \varepsilon_0$. In this case equation (3.11) factors

$$(y^2 - d)(y^2 - \alpha_0 y + d) = 0. \tag{3.12}$$

The largest root is $y = \dfrac{1}{2}(\alpha_0 + \sqrt{\alpha_0^2 - 4d})$, provided $0 < d \le \alpha_0^2/4$. If $d > \alpha_0^2/4$, then the quartic has only two real roots $y = \pm\sqrt{d}$. Thus,

$$y(d) = \begin{cases} (\alpha_0 + \sqrt{\alpha_0^2 - 4d})/2, & d \le \alpha_0^2/4, \\ \sqrt{d}, & d > \alpha_0^2/4. \end{cases}$$

[4]Technically, at the W-points there could be other, not necessarily diagonal critical states, however, by continuity, the diagonal critical points would still deliver the global minimum of $\Psi(\boldsymbol{F})$.

Now,

$$\phi(d) = \min_{y\in\mathbb{R}}\{\Phi_0(d/y, y) + h(d) - md\}, \quad \Phi_0(x, y) = \frac{\mu}{2}(x^2 + y^2) - \alpha x - \beta y$$

Therefore,

$$\phi'(d) = \frac{1}{y(d)}\frac{\partial\Phi_0}{\partial x}(d/y, y) + h'(d) - m = \mu\frac{d - \alpha_0 y(d)}{y(d)^2} + h'(d) - m.$$

In the case of W-points for which $y(d)$ solves (3.12) we see that

$$\frac{d - \alpha_0 y(d)}{y(d)^2} = -1$$

when $d \le \alpha_0^2/4$. Hence, any critical point of $\phi(d)$ in this regime would have to satisfy

$$h'(d) - \mu - m = 0.$$

One of the solutions is d_-, which always satisfies $d_- \le \alpha_0^2/4$. If this equation has 3 solutions, the middle one corresponds to a local maximum of $\phi(d)$, while the third $d^* > d_+$ always fails to satisfy $d^* \le \alpha_0^2/4$ because $d_+ = \varepsilon_0^2 > (\varepsilon_- + \varepsilon_0)^2/4$, due to (3.8). We conclude that the only critical points of $\phi(d)$ that need to be checked are the ones that satisfy $d > \alpha_0^2/4$. In this regime $y(d)^2 = d$, and

$$\phi'(d) = \mu\left(1 - \frac{\alpha_0}{\sqrt{d}}\right) + h'(d) - m.$$

Observe that $\phi'(d) > 0$ when $d \ge \max(\alpha_0^2, \widetilde{d}_+)$, where $\widetilde{d}_+$ is the largest root of $h'(d) - m$. Hence we only need to check for critical points in a specific bounded interval. In fact, if $h(d)$ is given by (3.2), then it is easy to see that $\phi'(d) > 0$ for all $d \ge \alpha_0^2$. Hence, we only need to check for critical points of $\phi(d)$ on $(\alpha_0^2/4, \alpha_0^2)$. In addition, since $\{\!\{h'\}\!\} = 0$, for $h(d)$ given by (3.2), we have $m = -\mu\{\!\{\varepsilon\}\!\}/\varepsilon_0 = -\mu\alpha_0/(2\varepsilon_0)$. Thus, we obtain the following characterization of polyconvexity of W-points.

THEOREM **3.1.** *Let $h(d)$ be given by (3.2), then W-points are polyconvex whenever*

$$\min_{d\in\left[\frac{\alpha_0^2}{4},\alpha_0^2\right]}\left(h(d) + \mu\left(d + \frac{\alpha_0 d}{2\varepsilon_0} - 2\alpha_0\sqrt{d}\right)\right) = h(\varepsilon_0^2) - \mu\varepsilon_0\left(\frac{\varepsilon_0}{2} + \frac{3\varepsilon_-}{2}\right). \tag{3.13}$$

where $\alpha_0 = \varepsilon_0 + \varepsilon_-$, with $(\varepsilon_0, \varepsilon_-)$, $(\varepsilon_-, \varepsilon_0)$, and $(\varepsilon_0, \varepsilon_0)$ being the coordinates of W-points.

The right-hand side in (3.13) is just $\phi(\varepsilon_0^2)$, where $\phi(d)$ is the function being minimized in (3.13). For quartic energy (3.2) we compute the coordinates of W-points by solving

$$-4d(d - d_1)(d - d_2) = \mu.$$

Then ε_0^2 is the largest root, and

$$\varepsilon_- = \frac{d_1 + d_2 - \varepsilon_0^2}{\varepsilon_0}.$$

We can compute the largest value of μ for which (3.13) holds by substituting $\mu = -4\varepsilon_0^2(\varepsilon_0^2 - d_1)(\varepsilon_0^2 - d_2)$ into (3.13) and regarding $\varepsilon_0 \leq \sqrt{d_2}$ as a parameter. When $\varepsilon_0 = \sqrt{d_2}$, $\phi(d) - \phi(d_2)$ is a positive polynomial in $x = \sqrt{d}$. We then seek numerically the largest value of $\varepsilon_0 < \sqrt{d_2}$ for which the polynomial $P(x) = (\phi(x^2) - \phi(\varepsilon_0^2))/(x - \varepsilon_0)^2$ develops a double root. Algebraically this means seeking the largest root $\varepsilon_0 < \sqrt{d_2}$ of the discriminant. This solution gives the largest value of μ below which the W-points are polyconvex. For example, when $d_1 = 1$, $d_2 = 3$, we have polyconvexity of W-points for all $\mu < 6.35888$. When μ increases past that value it enters a regime where the W-points are no longer polyconvex, but could still be quasiconvex. Increasing μ even further, we enter a regime where W-points fail a more sophisticated stability test from [26]. The exact value of μ, where W-points stop being stable is unknown. In this paper we are working exclusively in the regime of sufficiently small μ, when W-points are polyconvex.

Secondary jump set. For general values of μ the algebraic equations (2.7) describing the secondary jump set can be solved only numerically. By contrast, when μ is small, the asymptotics of the solutions can be obtained explicitly, providing an excellent approximation to the computed secondary jump set for $\mu < 3$, with $d_1 = 1$, $d_2 = 3$. While the entire secondary jump set is unstable, as will be proved in [30], we will see that it provides an excellent (inside) bound for the binodal. Here we specialize general equations (2.7) to the specific energy density (3.1) without assuming that the rigidity measure μ is small.

Suppose that $\boldsymbol{F}_0$ lies on the secondary jump set. Then there exists $\varepsilon_\pm$, ε_0 and $\lambda \in [0, 1]$, such that the pair $\boldsymbol{F}_0, \overline{\boldsymbol{F}}$, where

$$\overline{\boldsymbol{F}} = \begin{bmatrix} \overline{\varepsilon} & 0 \\ 0 & \varepsilon_0 \end{bmatrix}, \qquad \overline{\varepsilon} = \lambda\varepsilon_+ + (1-\lambda)\varepsilon_-,$$

satisfies the secondary jump set equations (2.7). We compute

$$\overline{\boldsymbol{P}} = \lambda \boldsymbol{P}_+ + (1-\lambda)\boldsymbol{P}_- = \begin{bmatrix} \mu\overline{\varepsilon} + \overline{h'}\varepsilon_0 & 0 \\ 0 & \mu\varepsilon_0 + \overline{\varepsilon h'} \end{bmatrix}.$$

We have

$$\boldsymbol{P}_0 = \mu\boldsymbol{F}_0 + h'(d_0)\mathrm{cof}\boldsymbol{F}_0 = \mu \begin{bmatrix} \overline{\varepsilon} & 0 \\ 0 & \varepsilon_0 \end{bmatrix} + \mu \boldsymbol{b} \otimes \boldsymbol{m} + h'(d_0) \left(\begin{bmatrix} \varepsilon_0 & 0 \\ 0 & \overline{\varepsilon} \end{bmatrix} + \boldsymbol{b}^\perp \otimes \boldsymbol{m}^\perp \right).$$

Thus, the second and the third equations in the secondary jump set system (2.7) become

$$\begin{cases} \begin{bmatrix} (h'(d_0) - \overline{h'})\varepsilon_0 & 0 \\ 0 & h'(d_0)\overline{\varepsilon} - \overline{\varepsilon h'} \end{bmatrix} \boldsymbol{m} = -\mu \boldsymbol{b}, \\ \begin{bmatrix} (h'(d_0) - \overline{h'})\varepsilon_0 & 0 \\ 0 & h'(d_0)\overline{\varepsilon} - \overline{\varepsilon h'} \end{bmatrix} \boldsymbol{b} = -\mu |\boldsymbol{b}|^2 \boldsymbol{m}. \end{cases}$$

These equations result in 3 possibilities:

(a) $(h'(d_0) - \overline{h'})\varepsilon_0 = h'(d_0)\overline{\varepsilon} - \overline{\varepsilon h'} = -\gamma$, $\mu \boldsymbol{b} = \gamma \boldsymbol{m}$, $\boldsymbol{m} \in \mathbb{S}^1$;

(b) $(h'(d_0) - \overline{h'})\varepsilon_0 = -(h'(d_0)\overline{\varepsilon} - \overline{\varepsilon h'}) = -\gamma$, $\mu \boldsymbol{b} = \gamma \boldsymbol{I}_- \boldsymbol{m}$, $\boldsymbol{I}_- = \begin{bmatrix} 1 & 0 \\ 0 & -1 \end{bmatrix}$, $\boldsymbol{m} \in \mathbb{S}^1$;

(c) $(h'(d_0) - \overline{h'})\varepsilon_0 \neq \pm(h'(d_0)\overline{\varepsilon} - \overline{\varepsilon h'})$.

Possibility (c) implies that $\boldsymbol{F}_0$ must be diagonal, and will be our main focus. In [30] it will be shown that in the cases (a) and (b) there are no solutions. Let us therefore assume that $\boldsymbol{F}_0$ is diagonal and has the form

$$\boldsymbol{F}_0 = \begin{bmatrix} x_0 & 0 \\ 0 & y_0 \end{bmatrix}.$$

This implies that $\overline{\boldsymbol{F}} - \boldsymbol{F}_0 = \beta \boldsymbol{e}_2 \otimes \boldsymbol{e}_2$. In particular

$$x_0 = \overline{\varepsilon} = \lambda \varepsilon_+ + (1-\lambda)\varepsilon_-, \quad \lambda \in (0,1).$$

Let us compute the diagonal matrices $\boldsymbol{P}_\pm$ using equations (3.4) and (3.5).

$$P_\pm^{11} = \mu\varepsilon_\pm + h'(d_\pm)\varepsilon_0 = \mu \{\!\{ \varepsilon \}\!\} = \frac{\mu(d_1+d_2)}{2\varepsilon_0}, \quad P_\pm^{22} = \mu\varepsilon_0 + h'(d_\pm)\varepsilon_\pm = \mu\left(\varepsilon_0 \mp \frac{[\![\varepsilon]\!]\varepsilon_\pm}{2\varepsilon_0}\right).$$

Let us compute the diagonal matrix $\boldsymbol{P}_0$.

$$P_0^{11} = \mu x_0 + h'(d_0)y_0 = \mu\overline{\varepsilon} + h'(d_0)\frac{d_0}{\overline{\varepsilon}}, \quad P_0^{22} = \mu y_0 + h'(d_0)x_0 = \frac{\mu d_0}{\overline{\varepsilon}} + h'(d_0)\overline{\varepsilon}.$$

Traction continuity equation $(\overline{\boldsymbol{P}} - \boldsymbol{P}_0)\boldsymbol{e}_2 = 0$ then becomes

$$\varepsilon_0 + \frac{[\![\varepsilon]\!]}{2\varepsilon_0}(\varepsilon_- - 2\lambda\{\!\{\varepsilon\}\!\}) - \frac{d_0}{\overline{\varepsilon}} - \frac{h'(d_0)}{\mu}\overline{\varepsilon} = 0.$$

It will be convenient to use $\overline{\varepsilon}$ as a variable in place of λ. Replacing λ above using $\overline{\varepsilon} = \varepsilon_- + \lambda[\![\varepsilon]\!]$ we obtain

$$\frac{d_0}{\overline{\varepsilon}} = \varepsilon_0 + \frac{1}{\varepsilon_0}(\varepsilon_+\varepsilon_- - \{\!\{\varepsilon\}\!\}\overline{\varepsilon}) - \frac{h'(d_0)}{\mu}\overline{\varepsilon}. \tag{3.14}$$

Let us now compute all the terms in the last equation in (2.7).

$$W(\boldsymbol{F}_0) = \frac{\mu}{2}(\overline{\varepsilon}^2 + y_0^2) + h(d_0) = \frac{\mu}{2}\left(\overline{\varepsilon}^2 + \frac{d_0^2}{\overline{\varepsilon}^2}\right) + h(d_0).$$

Next we compute

$$\overline{W} = W_- + \lambda[\![W]\!] = W_- + \lambda\mu[\![\varepsilon]\!]\{\!\{\varepsilon\}\!\} = W_- + \mu(\overline{\varepsilon} - \varepsilon_-)\{\!\{\varepsilon\}\!\},$$

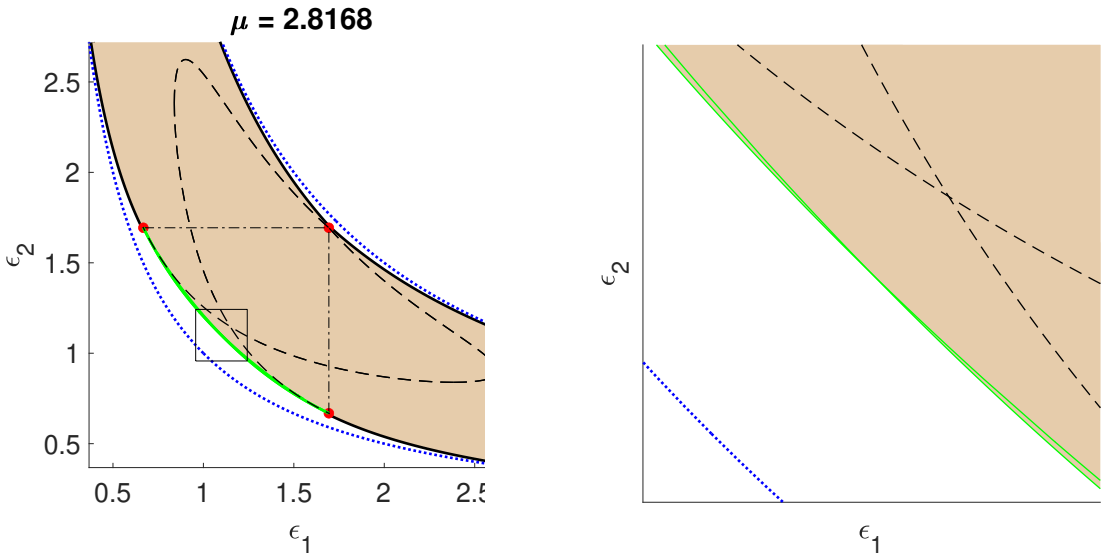

Figure 4: Secondary jump set (intersecting green lines) computed numerically from (3.14) and (3.15). The right panel shows the blown-up central box in the left panel.

where $[\![h]\!] = -\{\!\{h'\}\!\}[\![d]\!] = 0$ has been used. We compute

$$h(d_-) = [(d_- - d_1)(d_- - d_1)]^2 = \frac{\mu^2}{16\varepsilon_0^4},$$

according to (3.6). Therefore,

$$W_- = \frac{\mu}{2}(\varepsilon_-^2 + \varepsilon_0^2) + \frac{\mu^2}{16\varepsilon_0^4}.$$

We then compute $\boldsymbol{F}_0 - \overline{\boldsymbol{F}} = (y_0 - \varepsilon_0)\boldsymbol{e}_2 \otimes \boldsymbol{e}_2$. Therefore

$$\langle \overline{\boldsymbol{P}}, \boldsymbol{F}_0 - \overline{\boldsymbol{F}} \rangle = \mu \left(\frac{d_0}{\overline{\varepsilon}} - \varepsilon_0 \right) \left(\varepsilon_0 + \frac{1}{\varepsilon_0}(\varepsilon_+\varepsilon_- - \{\!\{\varepsilon\}\!\}\overline{\varepsilon}) \right).$$

Finally, the Maxwell equation $W(\boldsymbol{F}_0) - \overline{W} = \langle \overline{\boldsymbol{P}}, \boldsymbol{F}_0 - \overline{\boldsymbol{F}} \rangle$ can be written as

$$\frac{1}{2}\left(\overline{\varepsilon}^2 + \frac{d_0^2}{\overline{\varepsilon}^2}\right) + \frac{h(d_0)}{\mu} - (\overline{\varepsilon} - \varepsilon_-)\{\!\{\varepsilon\}\!\} - \frac{1}{2}(\varepsilon_-^2 + \varepsilon_0^2) - \frac{\mu}{16\varepsilon_0^4} = \left(\frac{d_0}{\overline{\varepsilon}} - \varepsilon_0 \right) \left(\varepsilon_0 + \frac{1}{\varepsilon_0}(\varepsilon_+\varepsilon_- - \{\!\{\varepsilon\}\!\}\overline{\varepsilon}) \right). \tag{3.15}$$

Next, in (3.15) we replace $d_0/\overline{\varepsilon}$ by its expression from (3.14). As a result of such substitution the Maxwell relation will also become a quadratic equation in $\overline{\varepsilon}$. This permits us to eliminate this variable as a rational expression in terms of ε_0 and d_0. The Maxwell relation will then reduce to a rational relation between d_0 and ε_0.

The implied calculation can only be done with the aid of a computer algebra system, since the remaining equation $F(\varepsilon_0, d_0) = 0$ is very long and complicated. For a given choice of numerical values of μ, d_1 and d_2 we can then solve $F(\varepsilon_0, d_0) = 0$ numerically and extract

the solutions which satisfy $\lambda \in [0,1]$. The result for $d_1 = 1$, $d_2 = 3$ and $\mu = \mu_{\text{top}}/3$ is shown as a green curve in Fig. 4. As we can see, it identifies all points between the green curve and the dashed lines of the primary jump set as a part of the binodal region—an improvement over the primary jump set bound.

As shown in the right panel of Fig. 4, the secondary jump set consists of two curves related by symmetry with respect to the bisector of the first quadrant. Each curve starts at a W-point and ends at a point (not marked) on the dashed part of the jump set. The endpoints of the secondary jump set correspond to the extreme values 0 and 1 of the volume fraction λ in (2.8) and must lie on the primary jump set. There are two possibilities. Either $\boldsymbol{F} \neq \overline{\boldsymbol{F}}$ or $\boldsymbol{F} = \overline{\boldsymbol{F}}$ at $\lambda = 0$ or 1. In the former case the limiting position $\boldsymbol{F}_+$ of $\overline{\boldsymbol{F}}$ is rank-one related to two different points on the jump set: $\boldsymbol{F}_-$ (layer normal $\boldsymbol{e}_1$) and $\boldsymbol{F}$ (layer normal $\boldsymbol{e}_2$). The W-point $\boldsymbol{F}_+$ is the only one with this property. All other points $\boldsymbol{F}_+$ on the jump set have a unique counterpart $\boldsymbol{F}_-$. In the latter case a detailed asymptotic analysis shows that that the common limit point of $\boldsymbol{F}$ and $\overline{\boldsymbol{F}}$ must achieve equality in the "Legendre-Hadamard for phase boundaries" inequality from [26]. When μ is small, this point lies on the dashed part of the jump set and is used in numerical calculations. The technical details of the analysis will be reported elsewhere. The sections of each of the two curves from the W-point to the bisector of the quadrant form a part of the boundary of the new shaded region of unstable points.

Circular nucleus. As we have already mentioned, the secondary jump set (shown in green in Fig. 4) is unstable [30]. That means that the corresponding bound on the binodal is not optimal. To improve this bound we can use another method of probing the binodal: nucleation of bounded equilibrium energy-neutral inclusions. We reiterate that the theory explaining why such nucleation tests probe the binodal was developed in [24].

In the case of the isotropic, objective energy (3.1) and a hydrostatic loading it would be natural to assume that the shape of an optimal precipitate is circular. The deformation gradient $\boldsymbol{F}_0$ inside a circular precipitate must be a constant hydrostatic field that jumps across the circular boundary of the inclusion to fields $\boldsymbol{F}(\boldsymbol{x})$. In order for such a configuration to be able to probe the binodal, $\boldsymbol{F}_0$ and $\boldsymbol{F}(\boldsymbol{x})$ must be corresponding pairs on the jump set. There is only one point on the jump set satisfying these requirements $\boldsymbol{F}_0 = \varepsilon_0^{\text{W}} \boldsymbol{I}_2$, where $(\varepsilon_0^{\text{W}}, \varepsilon_0^{\text{W}})$ is the W-point that lies on the quadrant bisector. As required, the field $\boldsymbol{F}_0$ is rank-one connected to an infinite family of fields

$$\boldsymbol{F}_{\boldsymbol{R}} = \boldsymbol{R} \begin{bmatrix} \varepsilon_-^{\text{W}} & 0 \\ 0 & \varepsilon_0^{\text{W}} \end{bmatrix} \boldsymbol{R}^T, \qquad \boldsymbol{R} \in SO(2),$$

where $(\varepsilon_-^{\text{W}}, \varepsilon_0^{\text{W}})$ is a coordinate of one of the other W-points. The deformation gradient outside of the circular inclusion must solve the Euler-Lagrange equation for the energy (3.1)

$$\mu \Delta \boldsymbol{y} + (\text{cof} \nabla \boldsymbol{y}) \nabla h'(\det \nabla \boldsymbol{y}) = 0, \qquad \boldsymbol{x} \in \mathbb{R}^2 \setminus B(\boldsymbol{0}, 1), \tag{3.16}$$

and agree with $\boldsymbol{F}_{\boldsymbol{R}}$ at the point $\boldsymbol{R}\boldsymbol{e}_1$ on the boundary of the circular inclusion:

$$\nabla \boldsymbol{y}(\boldsymbol{x}) = \varepsilon_-^{\text{W}} \boldsymbol{n} \otimes \boldsymbol{n} + \varepsilon_0^{\text{W}} \boldsymbol{n}^\perp \otimes \boldsymbol{n}^\perp, \qquad \boldsymbol{x} \in \partial B(\boldsymbol{0}, 1). \tag{3.17}$$

Under these conditions, both equations (2.9) will be satisfied for the possibly marginally stable matrix

$$\boldsymbol{F}_\infty = \lim_{|\boldsymbol{x}|\to\infty} \nabla \boldsymbol{y}(\boldsymbol{x}) = \varepsilon_\infty \boldsymbol{I}_2.$$

We also know that that the values of $\nabla \boldsymbol{y}(\boldsymbol{x})$ inside the circular inclusion and its trace on the outside boundary of the inclusion must be stable. Our results from [24] then say that there are two possibilities. The first one is that $\boldsymbol{F}_\infty$ lies on the binodal and all values $\nabla \boldsymbol{y}(\boldsymbol{x})$ in the exterior of the inclusion are stable. The second option is that $\boldsymbol{F}_\infty$ lies in the interior of the binodal region $\mathfrak{B}$.

In our special radially symmetric case we look for a radially symmetric solution of (3.16)

$$\boldsymbol{y} = \eta(r)\hat{\boldsymbol{x}}, \qquad |\boldsymbol{x}| > 1.$$

The unknown function $\eta(r)$ must solve

$$\begin{cases} \frac{\eta}{r}\frac{d}{dr} h' \left(\frac{\eta\eta'}{r}\right) + \mu \left(\eta' + \frac{\eta}{r}\right)' = 0, \quad r > 1, \\ \eta'(1) = \varepsilon_-^{\mathrm{W}}, \qquad \eta(1) = \varepsilon_0^{\mathrm{W}}. \end{cases} \tag{3.18}$$

The nonlinear second order ODE (3.18) cannot be integrated explicitly, but can be solved numerically. In order to do so, we need to convert the infinite range $r > 1$ into a finite one by means of the change of the independent variable $x = 1/r^2$. It will also be convenient to change the dependent variable $v = \eta/r$, so that $v(x)$ would have a finite limit, when $x \to 0$. Then $v(x)$ solves

$$v'' = -\frac{(v')^2 v h''(v^2 - 2xvv')}{\mu + v^2 h''(v^2 - 2xvv')}, \quad x \in [0,1], \quad v(1) = \varepsilon_0^{\mathrm{W}}, \quad v'(1) = \frac{\varepsilon_0^{\mathrm{W}} - \varepsilon_-^{\mathrm{W}}}{2}. \tag{3.19}$$

The value $\varepsilon_\infty = v(0)\boldsymbol{I}_2$, which was found numerically, is shown as a blue dot in Fig. 6. While we still cannot say whether the corresponding value $\boldsymbol{F}_\infty$ indeed lies on the binodal, we obtained an improved bound for the binodal compared to the secondary jump set (green line in Fig. 6) by showing that hydrostatic strains between the blue dot and the green line are unstable. The conclusion holds, provided the non-degeneracy condition (2.10) is verified. A direct calculation shows that

$$\int_{\mathbb{R}^2} W^\circ_{\boldsymbol{F}}(\boldsymbol{F}_0, \nabla\boldsymbol{\phi}) d\boldsymbol{x} = -\boldsymbol{I}_2 \int_{\mathbb{R}^2} h''(\varepsilon_\infty^2)\varepsilon_\infty^2 \left(\eta'(r) + \frac{\eta(r)}{r} - 2\varepsilon_\infty\right) d\boldsymbol{x}.$$

Thus,

$$\int_{\mathbb{R}^2} W^\circ_{\boldsymbol{F}}(\boldsymbol{F}_0, \nabla\boldsymbol{\phi}) d\boldsymbol{x} = -2\pi h''(\varepsilon_\infty^2)\varepsilon_\infty^2 \boldsymbol{I}_2 \lim_{r\to\infty} (r\eta(r) - \varepsilon_\infty r^2).$$

To see that the limit above exists and is non-zero, at least for sufficiently small $\mu > 0$, we simply solve (3.18) for $\mu = 0$, for which $\varepsilon_0^{\mathrm{W}} = \sqrt{d_2}$, $\varepsilon_-^{\mathrm{W}} = \frac{d_1}{\sqrt{d_2}}$. The solution is $\eta(r) = \sqrt{d_1 r^2 + d_2 - d_1}$, and we easily see that

$$\lim_{r\to\infty} (r\eta(r) - \varepsilon_\infty r^2) = \frac{d_2 - d_1}{2\sqrt{d_1}}.$$

Hence, the non-degeneracy condition (2.10) will hold for sufficiently small $\mu > 0$. The non-degeneracy will also hold for all μ below the topological transition, because if we write $\widetilde{\eta}(r) = \eta(r) - \varepsilon_\infty r$, then (assuming that $\widetilde{\eta}'(r) \to 0$, as $r \to \infty$) $\widetilde{\eta}(r)$ will solve, when r is large, the differential equation

$$\varepsilon_\infty h''(\varepsilon_\infty^2)\left(\varepsilon_\infty\left(\widetilde{\eta}' + \frac{\widetilde{\eta}}{r}\right) + \frac{\widetilde{\eta}'\widetilde{\eta}}{r}\right) + \mu\left(\widetilde{\eta}' + \frac{\widetilde{\eta}}{r}\right) = 0.$$

This integrates to

$$\varepsilon_\infty h''(\varepsilon_\infty^2)(2\varepsilon_\infty r\widetilde{\eta} + \widetilde{\eta}^2) + 2\mu r\widetilde{\eta} = 2c.$$

Since $\widetilde{\eta}$, satisfying $\widetilde{\eta}'(r) \to 0$, as $r \to \infty$, cannot be zero (it is the leading term of $\eta(r) - \varepsilon_\infty r$), we conclude that the constant of integration c cannot be zero either. Hence, we obtain that

$$\lim_{r\to\infty}(r\eta(r) - \varepsilon_\infty r^2) = \lim_{r\to\infty} r\widetilde{\eta}(r) = \frac{c}{\mu + \varepsilon_\infty^2 h''(\varepsilon_\infty^2)} \neq 0.$$

Polyconvexity limits along $\varepsilon \boldsymbol{I}_2$. In an attempt to prove stability of the point $\varepsilon_\infty \boldsymbol{I}_2$ we turn to the problem of polyconvexity at points $\boldsymbol{F} = \varepsilon \boldsymbol{I}_2$. The problem reduces to finding a constant $m \in \mathbb{R}$, such that (2.5) holds. For our energy we compute

$$W^\circ(\boldsymbol{F}, \boldsymbol{H}) = \frac{\mu}{2}|\boldsymbol{H}|^2 + h(\varepsilon^2 + d + \varepsilon\theta) - h(\varepsilon^2) - \varepsilon h'(\varepsilon^2)\theta, \qquad \theta = \operatorname{Tr}\boldsymbol{H},\ d = \det \boldsymbol{H}.$$

We also have

$$|\boldsymbol{H}|^2 = 4s^2 - 2d + \theta^2,$$

where

$$\frac{1}{2}(\boldsymbol{H} - \boldsymbol{H}^T) = \begin{bmatrix} 0 & -s \\ s & 0 \end{bmatrix}.$$

The set of all admissible values of (θ, d, s) is described by the inequality[5] $s^2 \geq d - \theta^2/4$. Thus, proving that $W^\circ(\varepsilon \boldsymbol{I}_2, \boldsymbol{H}) \geq m \det \boldsymbol{H}$ for all $\boldsymbol{H}$ is equivalent to proving that

$$2\mu \max\left\{0, d - \frac{\theta^2}{4}\right\} + \frac{\mu\theta^2}{2} + h(\varepsilon^2 + d + \varepsilon\theta) - h(\varepsilon^2) - \varepsilon h'(\varepsilon^2)\theta \geq (m + \mu)d.$$

Establishing this inequality splits into two cases

$$\frac{\mu\theta^2}{2} + h(\varepsilon^2 + d + \varepsilon\theta) - h(\varepsilon^2) - \varepsilon h'(\varepsilon^2)\theta \geq (m + \mu)d, \quad \forall d \leq \frac{\theta^2}{4}, \tag{3.20}$$

and

$$h(\varepsilon^2 + d + \varepsilon\theta) - h(\varepsilon^2) - \varepsilon h'(\varepsilon^2)\theta \geq (m - \mu)d, \quad \forall d \geq \frac{\theta^2}{4}. \tag{3.21}$$

In particular both inequalities must hold for $d = \theta^2/4$. In that case we must have

$$m \leq \mu + 4\min_{\theta\in\mathbb{R}} \frac{h(\varepsilon^2 + \theta^2/4 + \varepsilon\theta) - h(\varepsilon^2) - \varepsilon h'(\varepsilon^2)\theta}{\theta^2} = m^*. \tag{3.22}$$

[5]This inequality is equivalent to $|\operatorname{dev}(\boldsymbol{H})|^2 \geq 0$, where $2\operatorname{dev}(\boldsymbol{H}) = \boldsymbol{H} + \boldsymbol{H}^T - (\operatorname{Tr}\boldsymbol{H})\boldsymbol{I}_2$.

Changing variables $\delta = \varepsilon^2 + d + \varepsilon\theta$ we obtain that $\boldsymbol{F} = \varepsilon \boldsymbol{I}_2$ is polyconvex if and only if there exists $m \leq m_*$, such that

$$\inf_{\delta \leq (\varepsilon+\theta/2)^2} F_1(\delta, \theta) \geq 0, \quad F_1(\delta,\theta) = \frac{\mu\theta^2}{2} + h(\delta) - h(\varepsilon^2) - \varepsilon h'(\varepsilon^2)\theta - (m+\mu)(\delta - \varepsilon\theta - \varepsilon^2), \tag{3.23}$$

and

$$\inf_{\delta \geq (\varepsilon+\theta/2)^2} F_2(\delta, \theta) \geq 0, \quad F_2(\delta,\theta) = h(\delta) - h(\varepsilon^2) - \varepsilon h'(\varepsilon^2)\theta - (m-\mu)(\delta - \varepsilon\theta - \varepsilon^2). \tag{3.24}$$

The case (3.24) is clear, because $F_2(\delta, \theta)$ is linear in θ and the minimum is always achieved on the boundary of the admissible domain, i.e. $\delta = (\varepsilon + \theta/2)^2$ or, equivalently, $d = \theta^2/4$. In this case inequality (3.24) holds whenever $m \leq m^*$.

The function $F_1(\delta, \theta)$ is quadratic in θ and therefore achieves its minimal value either on the boundary, corresponding to $d = \theta^2/4$ or at the critical point, satisfying

$$\theta = \frac{\varepsilon(h'(\varepsilon^2) - m - \mu)}{\mu}, \quad h'(\delta) = m + \mu, \tag{3.25}$$

provided $\delta \leq (\theta/2 + \varepsilon)^2$, which holds if and only if

$$\delta \leq \frac{\varepsilon^2 (h'(\varepsilon^2) + \mu - m)^2}{4\mu^2}. \tag{3.26}$$

We remark that taking $\theta = -4\varepsilon$ in (3.22) we infer that $m^* \leq \mu + h'(\varepsilon^2)$. Thus, the right-hand side of (3.26) is monotone decreasing in m, when $m \leq m^*$.

Let $\widetilde{d}_1 < \widetilde{d}_2$ be the two inflection points of $h(d)$. The point $\widetilde{d}_1$ is the point of local maximum of $h'(d)$, while $\widetilde{d}_2$ is the point of local minimum of $h'(d)$. There are several cases, depending on the value of m^*.

- If $m^* + \mu > h'(\widetilde{d}_1)$, then equation $h'(\delta) = m^* + \mu$ has a unique solution δ^*. If $\delta = \delta^*$ fails (3.26) with $m = m^*$, then we have polyconvexity with $m = m^*$, since $F_1(\delta, \theta)$ has no critical points in $d < \theta^2/4$. If $\delta = \delta^*$ satisfies (3.26), then, if $f(\delta^*) \geq 0$, then polyconvexity holds with $m = m^*$. Here

$$f(\delta) = F_2(\delta, \theta(\delta)) = h(\delta) - h(\varepsilon^2) - h'(\delta)(\delta - \varepsilon^2) - \frac{\varepsilon^2 (h'(\delta) - h'(\varepsilon^2))^2}{2\mu}. \tag{3.27}$$

  If $f(\delta^*) < 0$, then we can try to find a better choice for $m < m^*$. In this case, all solutions δ of $h'(\delta) = m + \mu$ will be smaller than δ^* and therefore (3.26) will be satisfied for all roots of $h'(\delta) = m + \mu$, for any $m \leq m_*$. Polyconvexity will hold if $f(\delta) \geq 0$ for all roots of $h'(\delta) = m + \mu$ for some choice of $m \leq m^*$.

- If $m^* + \mu < h'(\widetilde{d}_2)$, then equation $h'(\delta) = m^* + \mu$ has a unique solution δ_*. If $\delta = \delta_*$ fails (3.26) with $m = m^*$, then we have polyconvexity with $m = m^*$, since in that case $F_1(\delta, \theta)$ has no critical points in $d < \theta^2/4$. If $\delta = \delta_*$ satisfies (3.26), then, for any $m \leq m^*$ there will be a unique solution δ of $h'(\delta) = m + \mu$, satisfying $\delta \leq \delta_*$. In this case polyconvexity fails if and only if $f(\delta) < 0$ for all $\delta < \delta_*$.

- If $m^* + \mu \in (h'(\widetilde{d}_2), h'(\widetilde{d}_1))$, then $h(\delta) = m^* + \mu$ has 3 real roots. If even the smallest root δ_* does not satisfy (3.26) with $m = m^*$, then polyconvexity holds, since $F_1(\delta, \theta)$ has no critical points. If the smallest root δ_* satisfies (3.26), then the smallest root of $h(\delta) = m + \mu$ will satisfy (3.26) for all $m \leq m^*$. Then, if $f(\delta) < 0$ for all $\delta \leq \delta_*$, polyconvexity fails. However, if there are values of $\delta \leq \delta_*$, such that $f(\delta) \geq 0$, then it does not imply polyconvexity. For polyconvexity to hold we must have $f(\delta) \geq 0$ for *all* roots of $h'(\delta) = m + \mu$, which satisfy (3.26).

More clarity regarding which case we need to deal with can be obtained in the limit $\mu \to 0$.

4 Limiting case $\mu \to 0$

In the previous section we have derived equations of the secondary jump set, conditions for polyconvexity of points $\varepsilon \boldsymbol{I}_2$ and a differential equation implicitly determining the nucleation bound $\varepsilon_\infty \boldsymbol{I}_2$. In the asymptotic limit $\mu \to 0$ these implicit conditions can be made explicit.

Secondary jump set. Expanding equation (3.7) to first order in μ we obtain

$$\varepsilon_+ = \frac{d_2}{\varepsilon_0} - \frac{\mu}{4\varepsilon_0^3(d_2 - d_1)} + O(\mu^2), \qquad \varepsilon_- = \frac{d_1}{\varepsilon_0} + \frac{\mu}{4\varepsilon_0^3(d_2 - d_1)} + O(\mu^2). \tag{4.1}$$

Since d_1 and d_2 are fixed, we consider the strains $\varepsilon_\pm$ as functions of ε_0 and μ, even if we suppress this in the notations. Clearly, when $\mu \to 0$ we have $\varepsilon_+ \to d_2/\varepsilon_0$, $\varepsilon_- \to d_1/\varepsilon_0$.

The parametric equations $(x_0(\varepsilon_0; \mu), y_0(\varepsilon_0; \mu))$ of secondary jump set converge, when $\mu \to 0$, to the hyperbola $x_0 y_0 = d_1$. In particular, $d_0(\varepsilon_0, \mu) \to d_1$, as $\mu \to 0$. The volume fraction λ of the rank-one laminate used in the second rank laminate is also a function of ε_0 and μ and must have a limit (at least along a subsequence) $\lambda(\varepsilon_0; \mu) \to \lambda_0(\varepsilon_0)$, as $\mu \to 0$. Equation (3.14) shows that $d_0 = d_1 + \mu\delta + O(\mu^2)$, where δ solves

$$\frac{\overline{d}}{\varepsilon_0}\left(\varepsilon_0 + \frac{1}{\varepsilon_0}\left(\frac{d_1}{d_2}\varepsilon_0^2 - \frac{d_1 + d_2}{2\varepsilon_0^2}\overline{d}\right)\right) - d_1 - 2\delta(d_2 - d_1)^2\frac{\overline{d}^2}{\varepsilon_0^2} = 0, \tag{4.2}$$

where $\overline{d} = \lambda d_2 + (1 - \lambda)d_1$. Equation (4.2) was obtained simply by passing to the limit as $\mu \to 0$ in equation (3.14).

When we pass to the limit as $\mu \to 0$ in (3.15) we obtain

$$\frac{(\overline{d} - d_1)^2(\varepsilon_0^4 + \overline{d}^2 - 2d_2\overline{d})}{2\varepsilon_0^2\overline{d}^2} = 0. \tag{4.3}$$

The dependence of $\overline{d}$ on the volume fraction λ is essential and should not disappear in the limit $\mu \to 0$. Therefore, the solution of (4.3) that we are after is

$$\overline{d} = d_2 - \sqrt{d_2^2 - \varepsilon_0^4}, \tag{4.4}$$

where the choice of the root was dictated by the requirement that $\overline{d} \leq d_2$. Combining this with the requirement that $\overline{d} \geq d_1$ we obtain the inequality

$$\sqrt[4]{d_2^2 - (d_2 - d_1)^2} \leq \varepsilon_0 \leq \sqrt{d_2}. \tag{4.5}$$

Substituting (4.4) into (4.2) we now can write the explicit formula for δ:

$$\delta = \frac{\varepsilon_0^4(d_2 - d_1) - 2(d_2^2 - \varepsilon_0^4)(d_2 - \sqrt{d_2^2 - \varepsilon_0^4})}{4\varepsilon_0^2(d_2 - d_1)^2(d_2 - \sqrt{d_2^2 - \varepsilon_0^4})^2}. \tag{4.6}$$

It looks as if in order to obtain the correct asymptotics of the secondary jump set we need to compute the first order asymptotics of $\overline{\varepsilon}$:

$$\overline{\varepsilon} = \frac{d_2 - \sqrt{d_2^2 - \varepsilon_0^4}}{\varepsilon_0} + \widetilde{\varepsilon}\mu + O(\mu^2). \tag{4.7}$$

In fact, this is not necessary because the leading order asymptotics of d_0 is *a constant* d_1. In that case, as far as the first order asymptotics as $\mu \to 0$ is concerned, using (4.7) simply corresponds to reparametrizing the curve

$$\begin{cases} x_0 = \dfrac{d_2 - \sqrt{d_2^2 - \varepsilon_0^4}}{\varepsilon_0}, \\ y_0 = \dfrac{d_1 + \mu\delta(\varepsilon_0)}{x_0}, \end{cases} \tag{4.8}$$

where the range of the parameter ε_0 along the secondary jump set is given in (4.5). Indeed, if we change the curve parameter ε_0 to $\varepsilon_0 + \mu\widetilde{\varepsilon}/x_0'(\varepsilon_0)$, then

$$x_0\left(\varepsilon_0 + \frac{\mu\widetilde{\varepsilon}}{x_0'(\varepsilon_0)}\right) = x_0(\varepsilon_0) + \mu\widetilde{\varepsilon} + O(\mu^2).$$

At the same time

$$y_0\left(\varepsilon_0 + \frac{\mu\widetilde{\varepsilon}}{x_0'(\varepsilon_0)}\right) = \frac{d_1}{x_0(\varepsilon_0)} - \frac{\mu d_1\widetilde{\varepsilon}}{x_0(\varepsilon_0)^2} + \frac{\mu\delta(\varepsilon_0)}{x_0(\varepsilon_0)} + O(\mu^2) = \frac{d_1 + \mu\delta}{x_0 + \mu\widetilde{\varepsilon}} + O(\mu^2).$$

We conclude that equation (4.8) correctly describes the asymptotics of the secondary jump set with $O(\mu^2)$ error, where the parameter ε_0 varies according to (4.5). When $\varepsilon_0 = \sqrt{d_2}$, the secondary jump set passes through one of the W-points. When $\varepsilon_0 = \sqrt[4]{d_2^2 - (d_2 - d_1)^2}$ it passes through the limiting point of the "Legendre-Hadamard for phase boundaries" bound (see [26]), that for small μ lies on the dashed part of the jump set in Fig. 4. The plot of (4.8) would be indistinguishable from the numerically obtained secondary jump set, if plotted in Fig. 4.

Circular nucleus. In the near-liquid limit $\mu \to 0$ we can find the asymptotics of the solution explicitly. We know that in the limit $\mu \to 0$ the field $d(\boldsymbol{x}) = \det \nabla \boldsymbol{y}(\boldsymbol{x})$ must approach d_1. Hence,

$$\frac{\eta\eta'}{r} = d_1 + \mu\delta(r) + O(\mu^2), \quad r > 1.$$

That implies

$$\eta(r) = \sqrt{d_1 r^2 + c_0} + \mu\widetilde{\eta}(r) + O(\mu^2), \tag{4.9}$$

and therefore,

$$\delta(r) = \frac{1}{r}\left(\widetilde{\eta}(r)\sqrt{d_1 r^2 + c_0}\right)'.$$

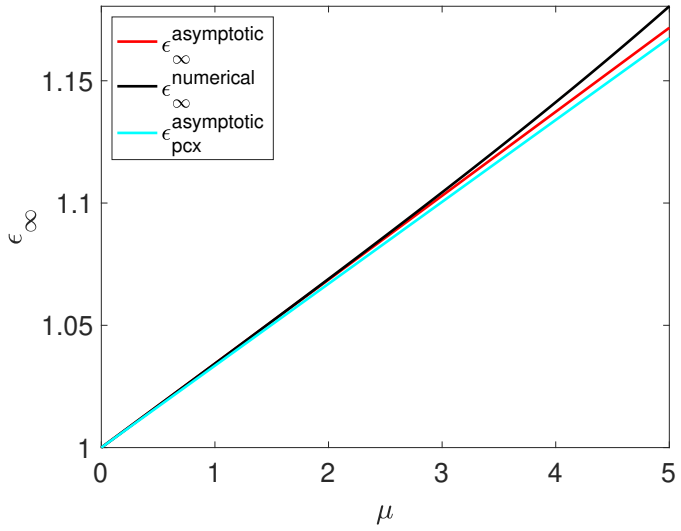

Figure 5: Comparison between the asymptotics (4.12) of ε_∞ (denoted here by $\varepsilon_\infty^{\text{asymptotic}}$) and $\varepsilon_\infty^{\text{numerical}}$ obtained from the numerical solution of (3.18). The plot also shows the asymptotics of ε_{pcx} (denoted here by $\varepsilon_{\text{pcx}}^{\text{asymptotic}}$), obtained from (4.16).

Substituting this ansatz into (3.18) we obtain

$$\mu\frac{\sqrt{d_1r^2+c_0}}{r}h''(d_1)\delta'(r)+\mu\left(\frac{d_1r}{\sqrt{d_1r^2+c_0}}+\frac{\sqrt{d_1r^2+c_0}}{r}\right)'+O(\mu^2)=0. \tag{4.10}$$

Initial conditions from (3.18) imply that

$$c_0=d_2-d_1,\quad \widetilde{\eta}(1)=-\frac{d_2-d_1}{4d_2^{3/2}h''(d_2)},\quad \widetilde{\eta}'(1)=\frac{d_1(d_2-d_1)}{2d_2^{3/2}}\left(\frac{1}{d_1h''(d_1)}+\frac{1}{2d_2h''(d_2)}\right).$$

Equation (4.10) is easy to integrate (observing that $\sqrt{d_1r^2+c_0}/r$ is decreasing from $\sqrt{d_2}$ to $\sqrt{d_1}$ and is therefore uniformly bounded away from zero and ∞).

$$h''(d_1)\widetilde{\eta}(r)=\frac{c_1r^2+c_2}{\sqrt{d_1r^2+c_0}}-\frac{r^2}{2\sqrt{d_1r^2+c_0}}\ln\frac{\sqrt{d_1r^2+c_0}}{r}. \tag{4.11}$$

From initial conditions for $\widetilde{\eta}(r)$ we obtain

$$c_1=\frac{1}{2}\ln\sqrt{d_2},\qquad c_2=-\frac{(d_2-d_1)h''(d_1)}{4d_2h''(d_2)},$$

and hence

$$\boldsymbol{\varepsilon}_\infty=\left(\sqrt{d_1}+\frac{\mu}{2h''(d_1)\sqrt{d_1}}\ln\frac{\sqrt{d_2}}{\sqrt{d_1}}\right)\boldsymbol{I}_2+O(\mu^2). \tag{4.12}$$

Figure 5 shows the quality of the asymptotics for the entire range of shear moduli μ. The numbers on the y-axis indicate that even for values of μ that are not particularly small the

asymptotics (4.12) gives a good approximation of the actual value of ε_∞. For example, for $\mu = 3$ the relative discrepancy is only around 0.1%.

Polyconvexity limits along $\varepsilon \boldsymbol{I}_2$. If $\mu = 0$, then we know that polyconvexity along $\varepsilon \boldsymbol{I}_2$ holds whenever $\varepsilon \notin [\sqrt{d_1}, \sqrt{d_2}]$. In this limiting case our analysis of polyconvexity applied to $\varepsilon = \sqrt{d_1}$ starts with the minimization problem (3.22), which simplifies[6]:

$$m \le \min_{\theta \in \mathbb{R}} \frac{h(d_1 + \theta\sqrt{d_1} + \theta^2/4)}{\theta^2} = 0 = m^*. \tag{4.13}$$

We first observe that in general $\theta = 0$ is not a minimizer. Then there are three minimizers:

$$\theta = -4\sqrt{d_1}, \qquad \theta = \pm 2\sqrt{d_2} - 2\sqrt{d_1}.$$

When μ is positive but small, we examine the polyconvexity of points $\varepsilon = \sqrt{d_1} + x$, where x is small. We know that as x increases, the polyconvexity will fail before $\varepsilon \boldsymbol{I}_2$ reaches the point on the secondary jump set, which is known to be unstable. Hence, we may regard the variable x to be of order μ, permitting us to compute the asymptotics of all quantities necessary to establish polyconvexity.

When $x > 0$, the minimizer $\theta(x)$ of (3.22) must be located near one of the three minimizers of (4.13). We can then write $\theta = \theta_0 + y$ for the minimizer, where θ_0 denotes one of the three. If we write the function under the minimum as $H(\varepsilon, \theta)$, then at the minimum we must have $\partial H/\partial\theta = 0$, which gives the equation

$$x\frac{\partial^2 H}{\partial\theta\partial\varepsilon} + y\frac{\partial^2 H}{\partial\theta^2} = 0$$

relating the infinitesimals x and y. After solving for y and substituting back into H we obtain

$$H = x\left(\frac{\partial H}{\partial\varepsilon} - \frac{\partial H}{\partial\theta}\frac{\dfrac{\partial^2 H}{\partial\theta\partial\varepsilon}}{\dfrac{\partial^2 H}{\partial\theta^2}}\right),$$

where derivatives are evaluated at $(\sqrt{d_1}, \theta_0)$. Maple calculation yields

$$H = \begin{cases} \frac{x}{2}\sqrt{d_1}h''(d_1), & \theta_0 = -4\sqrt{d_1}, \\ \frac{xd_1h''(d_1)}{\sqrt{d_1}+\sqrt{d_2}}, & \theta_0 = -2\sqrt{d_2} - 2\sqrt{d_1}, \\ \frac{xd_1h''(d_1)}{\sqrt{d_1}-\sqrt{d_2}}, & \theta_0 = 2\sqrt{d_2} - 2\sqrt{d_1}. \end{cases}$$

This shows that $\theta = 2\sqrt{d_2} - 2\sqrt{d_1} + y$ is the minimizer, while

$$m^* = \mu - \frac{4xd_1}{\sqrt{d_2} - \sqrt{d_1}}h''(d_1) + O(x^2).$$

In particular, the equation $h'(\delta) = m^* + \mu$ will have three real roots. Let us determine how many of them satisfy (3.26), which in the limit $\mu \to 0$, $x \to 0$ reads

$$\delta \le \left(d_1h''(d_1)\frac{\sqrt{d_1} + \sqrt{d_2}}{\sqrt{d_2} - \sqrt{d_1}}\frac{x}{\mu}\right)^2. \tag{4.14}$$

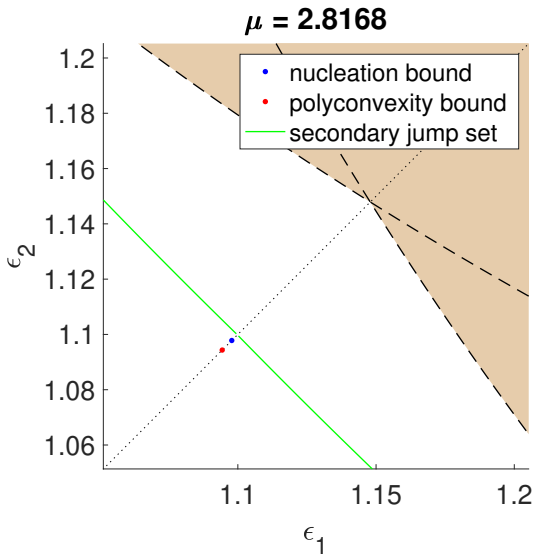

Figure 6: Bounds on the binodal from the inside and the outside of the binodal region along hydrostatic strains.

The smallest root δ_* of $h'(\delta) = m^* + \mu$ has the asymptotics

$$\delta_* = d_1 + \frac{\mu + m^*}{h''(d_1)} + O(\mu^2 + x^2).$$

Therefore, it will fail (4.14), when

$$x \leq \frac{\mu}{h''(d_1)\sqrt{d_1}} \frac{\sqrt{d_2} - \sqrt{d_1}}{\sqrt{d_2} + \sqrt{d_1}} + O(\mu^2). \tag{4.15}$$

If x is larger than the upper bound (4.15), then δ_* satisfies (4.14).

Let us now show that in this case $f(\delta) < 0$ for all $\delta \leq \delta_*$ for sufficiently small μ. Indeed, $h'(\delta)$ is a monotone increasing function on $\delta \leq \delta_*$. Therefore, either δ is close to d_1 or $h'(\delta) - h'(\varepsilon^2)$ is not small. In the latter case $f(\delta)$, given by (3.27) is clearly negative, as its last term tends to $-\infty$, when $\mu \to 0$. When δ is close to d_1, then, using the Taylor expansion of $h(\delta)$ centered at ε^2, we obtain

$$f(\delta) = -\frac{1}{2} h''(\varepsilon^2)(\delta - \varepsilon^2)^2 - \frac{\varepsilon^2 h''(\varepsilon^2)^2 (\delta - \varepsilon^2)^2}{2\mu} + O\left(\frac{(\delta - \varepsilon^2)^3}{\mu}\right),$$

which is obviously negative, when μ is sufficiently small. We conclude that polyconvexity at $\varepsilon \boldsymbol{I}_2$ holds when $\varepsilon \leq \varepsilon_{\rm pcx}$, where

$$\varepsilon_{\rm pcx} = \sqrt{d_1} + \frac{\mu}{h''(d_1)\sqrt{d_1}} \frac{\sqrt{d_2} - \sqrt{d_1}}{\sqrt{d_2} + \sqrt{d_1}} + O(\mu^2). \tag{4.16}$$

Our Fig. 6, where $\varepsilon_{\rm pcx} \boldsymbol{I}_2$ is represented by the red dot, shows that $\varepsilon_\infty \boldsymbol{I}_2$ fails to be polyconvex, but by a very slim margin. Our numerical investigations (to be reported elsewhere)

[6] We can assume. without loss of generality, that $h(d) \geq 0$ and $h(d) = 0$ only at $d = d_1$ and $d = d_2$.

shows that the ordering of the bounds in Fig. 6 persists on the entire range of μ. In Fig. 6 we see that the remaining gap between established stability (along the bisector below the red dot) and established instability (along the bisector above the blue dot) is very small.

5 A glimpse into the relaxed energy

Hypothetical bounds on the binodal. We have seen in the foregoing discussion that the energy $W(\boldsymbol{F})$ is not polyconvex at $\boldsymbol{F} = \varepsilon_\infty \boldsymbol{I}_2$. This is not very surprising, since polyconvexity is usually strictly stronger than quasiconvexity and we expect and conjecture that $\boldsymbol{F} = \varepsilon_\infty \boldsymbol{I}_2$ lies on the binodal—at the very edge of quasiconvexity.

First, we recall our observation that if $\boldsymbol{F} = \varepsilon_\infty \boldsymbol{I}_2$ is stable, then for every $|\boldsymbol{x}| > 1$ the deformation gradients

$$\nabla \boldsymbol{y}(\boldsymbol{x}) = \eta'(r)\hat{\boldsymbol{x}} \otimes \hat{\boldsymbol{x}} + \frac{\eta(r)}{r}(\boldsymbol{I}_2 - \hat{\boldsymbol{x}} \otimes \hat{\boldsymbol{x}})$$

are also stable in the sense of Definition 2.2. This observation would then provide a bound on the whole binodal from the outside.

Note next that for the entire range of μ for which W-points are polyconvex the union of the curves

$$\begin{cases} \varepsilon_1 = \frac{\eta(r)}{r}, \\ \varepsilon_2 = \eta'(r), \end{cases} \quad \text{and} \quad \begin{cases} \varepsilon_1 = \eta'(r) \\ \varepsilon_2 = \frac{\eta(r)}{r}, \end{cases} \qquad r > 1 \tag{5.1}$$

appear as almost indistinguishable from the secondary jump set curves shown in green in Fig. 4. This is more clear in Fig. 7 showing the blown-up part of the strain space from Fig. 6, where the curves (5.1) shown in magenta are meeting at the blue point from Fig. 6 entering it with slope -1. Assuming the conjectured stability of $\varepsilon_\infty \boldsymbol{I}_2$, the magenta curve must lie outside of the binodal region, while the secondary jump set lies in its interior. Thus, the binodal of the energy (3.1) would have to lie between the green and the magenta curves. We conjecture that the magenta curve is in fact the actual binodal of the energy (3.1). Independently of whether this more general conjecture is true, the magenta line represents a rather tight outside bound on the binodal region which hinges only on a more modest assumption of the stability of $\varepsilon_\infty \boldsymbol{I}_2$.

Another byproduct of the assumed stability of $\varepsilon_\infty \boldsymbol{I}_2$ would be the formula for the quasiconvex envelope $QW(\boldsymbol{F})$ for hydrostatic strains $\boldsymbol{F}$. If $\boldsymbol{F} = \varepsilon_\infty \boldsymbol{I}_2$ is stable, then our radial solution $\nabla \boldsymbol{y}(\boldsymbol{x}) = \eta(r)\hat{\boldsymbol{x}}$ of (3.18) is also a global minimizer in every finite ball $B(0, R)$, where it satisfies the affine boundary condition $\boldsymbol{y}(\boldsymbol{x}) = (\eta(R)/R)\boldsymbol{x}$, $\boldsymbol{x} \in \partial B(0, R)$ [29]. The energy of such configurations must necessarily be $QW(\eta(R)\boldsymbol{I}_2/R)|B(0, R)|$. This permits us to compute $QW(\varepsilon \boldsymbol{I}_2)$ for all ε, as the energy of configurations $\boldsymbol{y}(\boldsymbol{x}) = \eta(r)\hat{\boldsymbol{x}}$ in $B(0, R)$. Using the Clapeyron-type formula for the nonlinear elastic energy stored in an equilibrium stationary configuration we obtain for $\boldsymbol{F} = \eta(R)\boldsymbol{I}_2/R$: [29].

$$|B(0, R)|QW(\boldsymbol{F}) = \frac{1}{2}\int_{\partial B(0,R)} \{\boldsymbol{P}(\nabla \boldsymbol{y})\boldsymbol{n} \cdot \boldsymbol{y} + \boldsymbol{P}^*(\nabla \boldsymbol{y})\boldsymbol{n} \cdot \boldsymbol{x}\} dS. \tag{5.2}$$

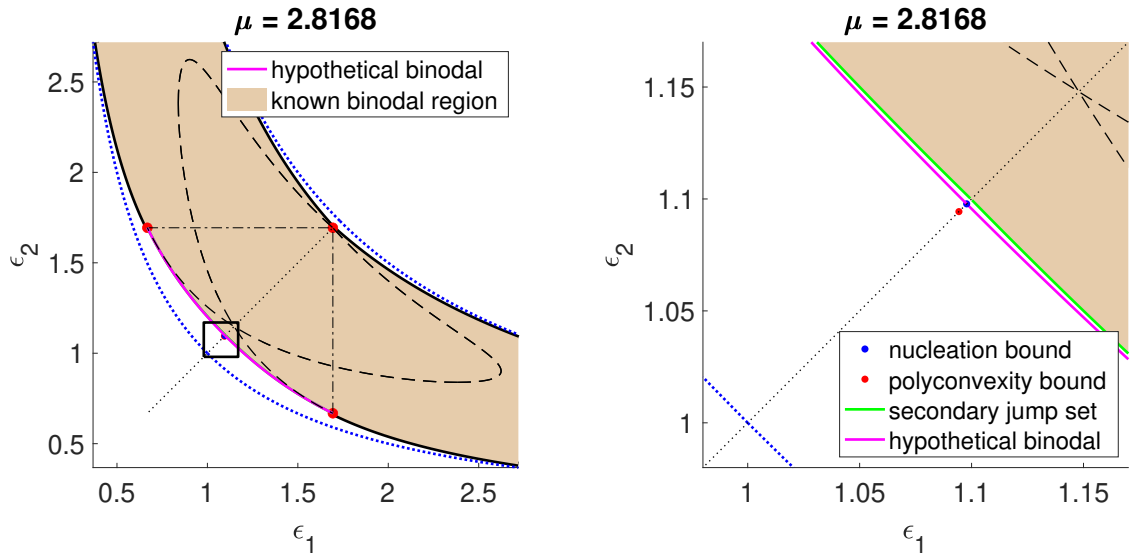

Figure 7: A hypothetical bound on the binodal region from the outside under the condition of stability of $\varepsilon_\infty \boldsymbol{I}_2$. The right panel is the blow-up of the square in the left panel.

Finally, substituting $\boldsymbol{n} = \hat{\boldsymbol{x}}$, $\boldsymbol{y} = \eta(r)\hat{\boldsymbol{x}}$ into (5.2) we obtain

$$QW\left(\frac{\eta(R)}{R}\boldsymbol{I}_2\right) = 2(\mu - h'(d))d - \mu\eta'(R)^2 + (2h'(d) + \mu)\frac{\eta(R)^2}{R^2} + 2h(d), \tag{5.3}$$

where

$$d = \frac{\eta'(R)\eta(R)}{R}.$$

When μ is small we can use the asymptotic formulas (4.9), (4.11) for $\eta(r)$ to obtain explicit asymptotics $QW^{\text{asym}}(\varepsilon \boldsymbol{I}_2)$ for $QW(\varepsilon \boldsymbol{I}_2)$. The plot of $QW(\varepsilon \boldsymbol{I}_2)$, coming from the numerical solution of (3.18), as well as its explicit asymptotic approximation $QW^{\text{asym}}(\varepsilon \boldsymbol{I}_2)$, superposed on the plot of $W(\varepsilon \boldsymbol{I}_2)$ are shown in Fig. 8.

6 Conclusions

In this paper we confronted the problem of solving analytically the relaxation problem for the double well Hadamard energy (3.1) in two space dimensions in the limit when the rigidity measure μ is sufficiently small. However, we only succeeded in attaining a much more modest goal of locating a substantial part of the corresponding binodal region in the strain space.

To deal analytically with these challenging questions, we used some of our previously developed methods centered around the computation of the jump set and the identification of its stable part. While our general methods apply for Hadamard materials in the entire parameter range and are amenable to numerical implementation, in this paper we have chosen to focus only on explicit asymptotic study of the "near-liquid" regime.

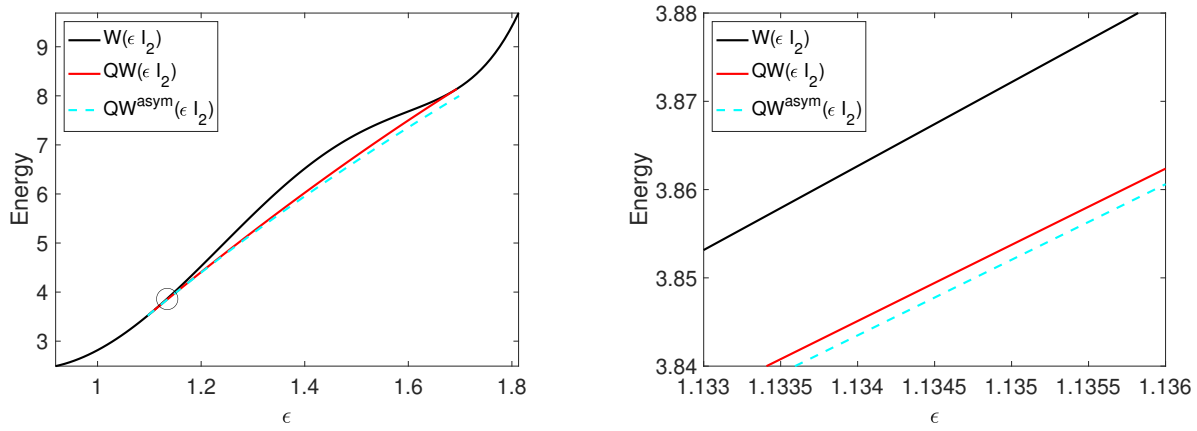

Figure 8: Quasiconvex envelope of $W(\boldsymbol{F})$ restricted to hydrostatic strains $\boldsymbol{F} = \varepsilon \boldsymbol{I}_2$. The right panel shows the blow-up of a subset of the small circle in the left panel.

In particular, we managed to show that in this limit, a subset of the jump set adjacent to the high strain phase remains stable which ensures that simple lamination delivers the corresponding part of the binodal. This means that even when the parameter μ is infinitesimally small, the high strain phase maintains its tangential rigidity at the level which ensures solid-solid like nature of the incipient phase transition.

By contrast, our analysis showed that the subset of the jump set adjacent to the low strain and low energy phase is unstable in the $\mu \to 0$ limit. Moreover, the secondary jump set is also unstable in this limit. This result implies that laminates of any *finite* rank are unstable and cannot be associated to any part of the binodal in that regime.

Whether the revealed asymmetry of the transformation mechanism between the direct and reverse transformation is a peculiarity of the Hadamard material or whether this striking phenomenon has a more general nature, remains to be established. It shows, however, the intricate role of rigidity in structural transformations which, even if weak, can produce complex microstructural morphologies underlying the relaxed energy. This complexity shows that, rather remarkably, the elastic long-range interactions remain relevant even when the system is arbitrarily close to the liquid regime. In other words, the disappearing rigidity can be viewed as the microstructure selection mechanism for the Hadamard liquid which otherwise comes with an infinite repertoire of possible accommodation mechanisms all having zero energetic cost.

In order to reconcile the solid-like features of the behavior of the near-liquid material with the behavior of its purely "liquid" limit one can turn from the study of global minima of the energy to the study of almost-minimizers whose energy is only slightly above the energy of the ground state. In this case the richness of the repertoire of purely liquid microstructures corresponding to $\mu = 0$ is expected to be recovered in the form of such almost-minimizers of the Hadamard solid with μ sufficiently small but finite. The physical merit of these projections must be weighed against other factors that have been neglected in our study, such as surface energy, crystal anisotropy, spatial inhomogeneity and dynamics.

A Calculation of the jump set for Hadamard materials

Here we recall the calculation of the jump set from [27] for energies (3.1).

We start with the first equation in (2.3) expressing the kinematic compatibility of the deformation gradients $\boldsymbol{F}_+$ and $\boldsymbol{F}_-$. Taking the determinant of both sides we obtain

$$d_+ = d_- + \operatorname{cof}\boldsymbol{F}_-\boldsymbol{n}\cdot\boldsymbol{a}, \quad d_\pm = \det\boldsymbol{F}_\pm. \tag{A.1}$$

Using the formula

$$\boldsymbol{P}(\boldsymbol{F}) = \mu\boldsymbol{F} + h'(\det\boldsymbol{F})\operatorname{cof}\boldsymbol{F}$$

for the Piola-Kirchhoff stress we compute

$$[\![\boldsymbol{P}]\!]\boldsymbol{n} = \mu\boldsymbol{a} + [\![h']\!]\operatorname{cof}\boldsymbol{F}_-\boldsymbol{n},$$

where we have used the well-known relation $\operatorname{cof}(\boldsymbol{F}_- + \boldsymbol{a}\otimes\boldsymbol{n})\boldsymbol{n} = (\operatorname{cof}\boldsymbol{F}_-)\boldsymbol{n}$. Similarly,

$$[\![\boldsymbol{P}]\!]^T\boldsymbol{a} = \mu|\boldsymbol{a}|^2\boldsymbol{n} + [\![h']\!]\operatorname{cof}\boldsymbol{F}_-^T\boldsymbol{a}.$$

Thus, the second and the third equations in (2.3) become

$$\boldsymbol{a} = -\frac{[\![h']\!]}{\mu}\operatorname{cof}\boldsymbol{F}_-\boldsymbol{n}, \qquad [\![h']\!]^2\operatorname{cof}(\boldsymbol{C}_-)\boldsymbol{n} = \mu^2|\boldsymbol{a}|^2\boldsymbol{n}, \tag{A.2}$$

where $\boldsymbol{C}_\pm = \boldsymbol{F}_\pm^T\boldsymbol{F}_\pm$ is the Cauchy-Green strain tensor. We conclude that $\boldsymbol{n}$ must be an eigenvector of $\boldsymbol{C}_-$. Equations (A.2) permit us to find a relation between the two Cauchy-Green tensors $\boldsymbol{C}_\pm$. Using the kinematic compatibility equation $(2.3)_1$ we compute

$$\boldsymbol{C}_+ = \boldsymbol{C}_- + \boldsymbol{F}_-^T\boldsymbol{a}\otimes\boldsymbol{n} + \boldsymbol{n}\otimes\boldsymbol{F}_-^T\boldsymbol{a} + |\boldsymbol{a}|^2\boldsymbol{n}\otimes\boldsymbol{n}.$$

Applying $\boldsymbol{F}_-^T$ to the first equation in (A.2) we obtain $\boldsymbol{F}_-^T\boldsymbol{a} = -([\![h']\!]/\mu)d_-\boldsymbol{n}$, so that

$$[\![\boldsymbol{C}]\!] = \left(|\boldsymbol{a}|^2 - \frac{2[\![h']\!]d_-}{\mu}\right)\boldsymbol{n}\otimes\boldsymbol{n}. \tag{A.3}$$

It follows that the Cauchy-Green tensors $\boldsymbol{C}_+$ and $\boldsymbol{C}_-$ are simultaneously diagonalizable, since, by (A.2) $\boldsymbol{n}$ is an eigenvector of $\boldsymbol{C}_-$. According to equation (A.3) symmetric matrices $\boldsymbol{C}_+$ and $\boldsymbol{C}_-$ have the same pair of mutually orthogonal eigenvectors $\boldsymbol{n}$ and $\boldsymbol{n}^\perp$ with the same eigenvalues corresponding to $\boldsymbol{n}^\perp$. Hence, singular values of $\boldsymbol{F}_\pm$ would be $(\varepsilon_\pm, \varepsilon_0)$, the first one corresponding to the eigenvector $\boldsymbol{n}$ of $\boldsymbol{C}_\pm$. Substituting the first equation in (A.2) into (A.1) we obtain

$$d_+ = d_- - \frac{[\![h']\!]}{\mu}\operatorname{cof}\boldsymbol{C}_-\boldsymbol{n}\cdot\boldsymbol{n} = d_- - \frac{[\![h']\!]d_-^2}{\mu\varepsilon_-^2},$$

which can be written in the more symmetric form as

$$\mu\frac{[\![d]\!]}{[\![h']\!]} = -\varepsilon_0^2 = -\frac{d_\pm^2}{\varepsilon_\pm^2}. \tag{A.4}$$

This will be the equation for the jump set, when we determine d_+ as a function of d_- from the Maxwell relation (the last equation in (2.3), which hasn't been used so far). It is well-known that the Maxwell relation does not change if we add any quadratic function of $\boldsymbol{F}$ to the energy. Thus, the term $\mu|\boldsymbol{F}|^2/2$ can be disregarded and the Maxwell relation becomes

$$[\![h]\!] = \{\!\{h' \mathrm{cof} \boldsymbol{F}\}\!\} \boldsymbol{n} \cdot \boldsymbol{a}.$$

Recalling that due to (A.1) $(\mathrm{cof}\boldsymbol{F}_+)\boldsymbol{n} \cdot \boldsymbol{a} = (\mathrm{cof}\boldsymbol{F}_-)\boldsymbol{n} \cdot \boldsymbol{a} = [\![d]\!]$ we obtain

$$[\![h]\!] = \{\!\{h'\}\!\}[\![d]\!]. \tag{A.5}$$

Equation (A.5) has a geometric meaning. It says that the secant line joining $(d_-, h'(d_-))$ and $(d_-, h'(d_-))$ together with the graph of $h'(d)$ bound two regions of equal areas. For a double-well shaped potential $h(d)$ there exists a single interval (d_1, d_2) on which $h(d)$ differs from its convex hull, which on (d_1, d_2) agrees with the common tangent line at d_1 and d_2 to the graph of $h(d)$. In terms of $h'(d)$ this double-tangency can also be interpreted geometrically as the horizontal "Maxwell line" with the equal area property. In that case there exist $d_0 \in (d_1, d_2)$, such that for any $d_- \in (d_1, d_0)$ there is a unique $d_+ \in (d_0, d_2)$ satisfying (A.5). In other words, for every $d_- \in (d_1, d_0)$ there is a unique $d_+ = D(d_-)$ with equal area property. (By continuity we can set $D(d_0) = d_0$.) Regarding the function $D(d)$ as known, equation (A.4) provides the explicit description of the jump set in terms of the singular values of $\boldsymbol{F}_\pm$.

Funding. YG was supported by the National Science Foundation under Grant No. DMS-2005538. The work of LT was supported by the French grant ANR-10-IDEX-0001-02 PSL.

Author contributions. The authors conducted the research and wrote the manuscript together

Declarations

Competing interests. The authors declare no competing interests.

References

[1] G. Allaire and R. V. Kohn. Explicit optimal bounds on the elastic energy of a two-phase composite in two space dimensions. *Quart. Appl. Math.*, LI(4):675–699, December 1993.

[2] Mikhail A. Antimonov, Andrej Cherkaev, and Alexander B. Freidin. Phase transformations surfaces and exact energy lower bounds. *International Journal of Engineering Science*, 90:153–182, 2016.

[3] J. M. Ball. Progress and puzzles in nonlinear elasticity. In Jörg Schröder and Patrizio Neff, editors, *Poly-, Quasi- and Rank-One Convexity in Applied Mechanics*, pages 1–15. Springer Vienna, Vienna, 2010.

[4] J. M. Ball and F. Murat. $W^{1,p}$-quasiconvexity and variational problems for multiple integrals. *J. Funct. Anal.*, 58(3):225–253, 1984.

[5] J.M. Ball and R.D. James. Incompatible sets of gradients and metastability. *Archive for Rational Mechanics and Analysis*, 218(3):1363–1416, 2015.

[6] John M. Ball. Some open problems in elasticity. In *Geometry, mechanics, and dynamics*, pages 3–59. Springer, New York, 2002.

[7] D. M. Barnett, J. K. Lee, H. I. Aaronson, and K. C. Russel. The strain energy of a coherent ellipsoidal precipitate. *Scripta Metall.*, 8:1447–1450, 1974.

[8] Paul M Chaikin, Tom C Lubensky, and Thomas A Witten. *Principles of condensed matter physics*, volume 10. Cambridge university press Cambridge, 1995.

[9] Isaac Chenchiah and Kaushik Bhattacharya. The relaxation of two-well energies with possibly unequal moduli. *Arch. Rat. Mech. Anal.*, 187(3):409–479, 2008.

[10] Philippe G Ciarlet. *Mathematical elasticity: Three-dimensional elasticity*. SIAM, 2021.

[11] B. Dacorogna. A relaxation theorem and its application to the equilibrium of gases. *Arch. Rational Mech. Anal.*, 77(4):359–386, 1981.

[12] B. Dacorogna. Quasiconvexity and relaxation of nonconvex problems in the calculus of variations. *J. Funct. Anal.*, 46(1):102–118, 1982.

[13] B. Dacorogna. *Direct methods in the calculus of variations*. Springer-Verlag, New York, 2nd edition, 2008.

[14] Michelle M Driscoll, Bryan Gin-ge Chen, Thomas H Beuman, Stephan Ulrich, Sidney R Nagel, and Vincenzo Vitelli. The role of rigidity in controlling material failure. *Proceedings of the National Academy of Sciences*, 113(39):10813–10817, 2016.

[15] J. Ericksen. Some phase transitions in crystals. *Archive for Rational Mechanics and Analysis*, 73:99–124, 1980.

[16] J. L. Ericksen. Equilibrium of bars. *J. Elasticity*, 5(3–4):191–201, 1975.

[17] J. L. Ericksen. Twinning of crystals. I. In *Metastability and incompletely posed problems (Minneapolis, Minn., 1985)*, pages 77–93. Springer, New York, 1987.

[18] J. L. Ericksen. On kinematic conditions of compatibility. *Journal of Elasticity*, 26(1):65–74, 1991.

[19] J. L. Ericksen. Bifurcation and martensitic transformations in Bravais lattices. *J. Elasticity*, 28(1):55–78, 1992.

[20] J. Gibbs, Willard. On the equilibrium of heterogeneous substances. *Transactions of the Connecticut Academy*, III:108–248 and 343–524, 1873 and 1874.

[21] Leonardo Golubović and T. C. Lubensky. Nonlinear elasticity of amorphous solids. *Physical review letters*, 63(10):1082–1085, 1989.

[22] Y. Grabovsky. Bounds and extremal microstructures for two-component composites: A unified treatment based on the translation method. *Proc. Roy. Soc. London, Series A.*, 452(1947):945–952, 1996.

[23] Y. Grabovsky and L. Truskinovsky. Roughening instability of broken extremals. *Arch. Rat. Mech. Anal.*, 200(1):183–202, 2011.

[24] Y. Grabovsky and L. Truskinovsky. Marginal material stability. *Journal of Nonlinear Science*, 23(5):891–969, 2013.

[25] Yury Grabovsky and Lev Truskinovsky. Normality condition in elasticity. *Journal of Nonlinear Science*, 24(6):1125–1146, 2014.

[26] Yury Grabovsky and Lev Truskinovsky. Legendre-Hadamard conditions for two-phase configurations. *Journal of Elasticity*, 123(2):225–243, 2016.

[27] Yury Grabovsky and Lev Truskinovsky. Explicit relaxation of a two-well hadamard energy. *Journal of Elasticity*, 135(1-2):351–373, 2019.

[28] Yury Grabovsky and Lev Truskinovsky. When rank-one convexity meets polyconvexity: An algebraic approach to elastic binodal. *J. Nonlinear Sci.*, 28(1):229–253, 2019.

[29] Yury Grabovsky and Lev Truskinovsky. A class of nonlinear elasticity problems with no local but many global minimizers. *J. Elasticity*, 154(1):147–171, 2023.

[30] Yury Grabovsky and Lev Truskinovsky. Ubiquity of infinite rank laminates. *to be submitted*, In preparation.

[31] J. Hadamard. *Leçons sur la propagation des ondes et les équations de l'hydrodynamique.* Hermann, Paris, 1903.

[32] Fritz John. Plane elastic waves of finite amplitude. Hadamard materials and harmonic materials. *Communications on Pure and Applied Mathematics*, 19(3):309–341, 1966.

[33] V. Kardonski and Roitburd. On the shape of coherent precipitates. *Phys. Met. Metallurg. USSR*, 33:210–212, 1972.

[34] A. G. Khachaturyan. *Theory of structural transformation in solids.* Wiley, New York, 1983.

[35] Armen G Khachaturyan. Some questions concerning the theory of phase transformations in solids. *Soviet Phys. Solid State*, 8(9):2163–2168, 1967.

[36] R. V. Kohn. The relaxation of a double-well energy. *Continuum Mech. Thermodyn.*, 3:193–236, 1991.

[37] Martin Kružík and Tomáš Roubíček. *Mathematical methods in continuum mechanics of solids*. Springer, 2019.

[38] L. B. Kublanov and A. B. Freidin. Nuclei of a solid phase in a deformable material. *Prikl. Mat. Mekh.*, 52(3):493–501, 1988.

[39] Lev Davidovich Landau and Evgenii Mikhailovich Lifshitz. *Statistical Physics: Volume 5*, volume 5. Elsevier, 2013.

[40] J. K. Lee, D. M. Barnett, and H. I. Aaronson. The elastic strain energy of coherent ellipsoidal precipitates in anisotropic crystalline solids. *Metall. Trans. A*, 8A:963–970, 1977.

[41] J. C. Maxwell. On the dynamic evidence of the molecular composition of bodies. *Nature*, 11(279-280):357–359, 374–377, 1875.

[42] A. Pineau. Influence of uniaxial stress on the morphology of coherent precipitates during coarsening — elastic energy considerations. *Acta Metall.*, 24:559–564, 1976.

[43] Allen C Pipkin. Elastic materials with two preferred states. *The Quarterly Journal of Mechanics and Applied Mathematics*, 44(1):1–15, 1991.

[44] Miroslav Silhavy. *The mechanics and thermodynamics of continuous media*. Springer Science & Business Media, 2013.

[45] J.D. van der Waals. The equilibrium between a solid body and a fluid phase, especially in the neighbourhood of the critical state. In *KNAW, Proceedings*, volume 6, pages 1903–1904, 1903.